Applied Energy 399 (2025) 126511

Contents lists available at ScienceDirect

Applied Energy

journal homepage: www.elsevier.com/locate/apenergy

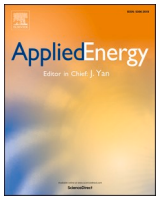

Comparative analysis of heating and cooling solutions for residential use: Energy, environmental, and economic perspectives

Mustafa Kurses [a], Andreas V. Olympios [b,c], Asmaa A. Harraz [d], Jingyuan Xu [a,*]

[a] Institute of Microstructure Technology, Karlsruhe Institute of Technology, Karlsruhe 76344, Germany
[b] PHAETHON Centre of Excellence for Intelligent, Efficient and Sustainable Energy Solutions, Nicosia, Cyprus
[c] PV Technology Laboratory, Department of Electrical and Computer Engineering, University of Cyprus, Nicosia, Cyprus
[d] Environmental Engineering Program, University of Science and Technology, Zewail City of Science and Technology, Egypt

HIGHLIGHTS

- 9 residential energy systems assessed in different European climate zones.
- Optimal system depends on local climate and energy price context.
- PV–heat pump system shows lowest LCOE across all climate zones.
- Solar-integrated systems reduce emissions and improve efficiency.
- Hydrogen boilers cut emissions but remain economically unviable.

ARTICLE INFO

Keywords:
Decarbonization pathways
Energy system modeling
Heating and cooling
Heat pumps
Renewable energy integration
Solar energy
Techno-economic analysis

ABSTRACT

This paper examines the techno-economic performance of domestic heating and cooling technologies across different climates. The novelty lies in the comprehensive assessment of a broad range of technological options using advanced thermodynamic and component-costing models. A holistic, like-for-like comparison is conducted for combinations of technologies that meet all residential energy needs – space heating, domestic hot water, space cooling, and electricity. Nine different system combinations are proposed, including natural gas boilers, photovoltaic systems, photovoltaic-thermal systems, solar thermal collectors, hydrogen boilers, air-to-water heat pumps, diffusion absorption refrigeration systems, and air-to-air air conditioners. These are analyzed for a typical single-family house under three distinct European climates: Athens (Greece), Strasbourg (France), and Helsinki (Finland), focusing on energy, economic, and environmental factors. From an economic perspective, the integrated photovoltaic - heat pump system configuration consistently has the lowest levelized cost of energy (LCOE) across all locations, ranging from 0.15 €/kWh in Athens to 0.20 €/kWh in Strasbourg. The photovoltaic-thermal – heat pump system configuration follows with a slightly higher LCOE than the photovoltaic – heat pump system (by 0.05–0.06 €/kWh) due to its higher initial costs. In general, solar integrated systems have an LCOE that is 0.10–0.20 €/kWh lower compared to the same systems that do not use solar energy. The payback time for the photovoltaic – heat pump system ranges from 4.65 years in Finland to 8.95 years in Greece. Standalone heat pump cost savings vary significantly and are lowest in Athens (403 €/year) and highest in Helsinki (2560 €/year) when compared to gas boilers, influenced by the regional electricity-gas price ratio, which is higher in Greece. However, photovoltaic and photovoltaic-thermal systems achieve a higher emission reduction in Athens (e.g., 4.70 tons of $CO_{2,eq}$/year for the photovoltaic – heat pump system), due to the carbon-intensive grid of Greece. Although hydrogen boilers show a high emission reduction in Strasbourg and Helsinki (4.27 tons of $CO_{2,eq}$/year), they exhibit higher LCOE than other systems (> 0.60 €/kWh), with their future viability depending on green hydrogen production costs. Overall, this study provides insights into residential energy systems across diverse climates, highlighting the importance of context-specific technology choices.

* Corresponding author.
E-mail address: jingyuan.xu@kit.edu (J. Xu).

https://doi.org/10.1016/j.apenergy.2025.126511
Received 13 April 2025; Received in revised form 10 June 2025; Accepted 17 July 2025
Available online 31 July 2025

Nomenclature

Acronyms

AC	Air conditioner
CO_2	Carbon dioxide
COP	Coefficient of performance (rate)
DAR	Direct absorption refrigeration
DHW	Domestic hot water
DSM	Demand-side management
EER	Energy efficiency ratio (rate)
EPCS	Environmental penalty cost savings (Euro)
ER	Emission reduction ($kgCO_2$)
GWP	Global warming potential ($kgCO_{2,eq}$)
HEX	Heat exchanger
HP	Heat pump
HTF	Heat transfer fluid
IRR	Internal rate of return (rate)
LCOE	Levelized cost of energy (Euro/kWh)
NGB	Natural gas boiler
NPV	Net present value (Euro)
PBT	Payback time (years)
PV	Photovoltaic
PVT	Photovoltaic thermal
SAHP	Solar-assisted heat pump
SC	Space cooling
SFH	Single-family house
SH	Space heating
ST	Solar thermal
TCS	Total cost saving

Symbols

A	Area (m^2)
C	Cost (€)
c_p	Specific heat capacity ($J\ kg^{-1}\ K^{-1}$)
d	Discount rate (rate)
D	Diameter (m)
G	Irradiance ($W\ m^{-2}$)
h_{conv}	Convective heat transfer coefficient ($W\ m^{-2}\ K^{-1}$)
H	Height (m)
HV	Heating value ($J\ kg^{-1}$)
I	Investment (€)
k	Thermal conductivity (W/m/K)
L	Length (m)
M	Mass (kg)
N	Number
Nu	Nusselt number (−)
P	Power (W)
Pr	Prandtl number (−)
$\dot{Q}$	Heat flow (W)
R	Thermal resistance ($W\ m^{-2}$)
Ra	Rayleigh Number (−)
Re	Reynolds Number (−)
S	Surface area (m^2)
T	Temperature (K)

Greek symbols

α	Absorptivity (−)
β	Temperature coefficient (K^{-1})
η	Efficiency (%)
ε	Heat exchanger effectiveness (−)
λ	Thermal conductivity ($W\ m^{-1}\ K^{-1}$)
φ	Excess air ratio (−)

Subscripts

amb	Ambient
app	Appliance
aux	Auxiliary
cov	Covered
dem	Demand
el	Electrical
exc	Excess
eq	Equivalent
f	Fuel
fg	Flue gas
gen	Generated
ins	Insulation
lim	Limit
max	Maximum
min	Minimum
mod	Module
ng	Natural gas
prod	Production
ref	Reference
s	Saving
th	Thermal
uncov	Uncovered
WT	Water tank

1. Introduction

The building sector is a significant contributor to global energy consumption, accounting for 30 % of global final energy consumption. In 2022, it was responsible for approximately 10 gigatons of CO_2 emissions, corresponding to about 26 % of global energy-related emissions [1]. Addressing these emissions is critical to mitigating climate change and achieving global sustainability goals. Given the long lifetimes of heating and cooling technologies, current choices will affect emissions for years. To achieve carbon neutrality by 2050, new buildings must be carbon-neutral by 2028, requiring urgent and transformative action. [2] [3]. While improving energy efficiency, like better insulation, can reduce emissions, it won't fully cut them without transitioning away from fossil fuels. Thus, adopting advanced technologies, improving energy efficiency of heating and cooling systems, and increasing the share of renewable energy sources on-site are essential steps. This not only reduces energy demand but also helps to decarbonize the building sector.

In the European Union, space heating (SH) and domestic hot water (DHW) account for 78.4 % of residential energy demand [4], with 75 % sourced from fossil fuels, 19 % from renewables, and the rest from electricity [5]. Decarbonizing this sector is critical, and heat pump (HP) systems that transfer heat from a cold ambient source to a hotter space with an input of work less than the transferred heat [6], are gaining momentum. HPs already account for 12 % of global residential heating equipment sales, surpassing fossil fuel-based systems in some markets like France. Their market share is expected to double by 2035, supported by policies such as Norway's 2017 ban on fossil fuel heating installations [7], and Finland's 2035 carbon neutrality goal [8].

Hydrogen is another proposed solution to decarbonize residential heating, which produces only water when burned in a hydrogen boiler. It benefits from the potential for repurposing of the existing natural gas distribution infrastructure for hydrogen supply. However, transitioning existing natural gas infrastructure to transport hydrogen presents significant technical challenges due to hydrogen's distinct properties compared to natural gas. Existing steel pipelines, especially at high

pressures, are prone to hydrogen embrittlement, which accelerates crack propagation and degrades the material's mechanical properties. Solutions to combat this include applying an inner coating, implementing operational strategies like keeping pressures steady to prevent crack formation, and potentially using lower-grade, more ductile steel alloys. Re-coating might enable operation at pressures closer to those used for natural gas [9]. Hydrogen's properties, such as its high diffusivity and low molecular weight, increase the leakage risk compared to natural gas. Distribution networks, with older sections made of steel or cast iron may need to be replaced by polyethylene to mitigate leakage risk [10]. Additionally, hydrogen's high flammability necessitates enhanced leak detection systems and upgraded safety protocols [11]. Hydrogen's volumetric energy density is approximately one-third that of methane [12], requiring larger pipeline volumes or significantly higher compression efforts to transport equivalent energy content. This means that the investment and operational costs for hydrogen compressors are higher than for natural gas [12]. Given these challenges, this shift is expected to be gradual [11]. For example, Germany plans to initially blend up to 20 % hydrogen into the natural gas grid to address safety and technical challenges [13]. Research indicates that blending ratios of 20–30 % is generally considered achievable with minimal network changes, while 100% hydrogen transport requires comprehensive infrastructure upgrades [10]. At the building level, hydrogen can replace natural gas with minimal changes to existing systems. While the boiler designs require specific design adaptations, existing components (e.g., radiators) remain unchanged. Hydrogen is often categorized by colors that reflect the greenhouse gas emissions associated with its production [14]. Green hydrogen, produced via renewable-powered electrolysis, is emission-free at the point of use. However, its widespread adoption for residential heating is currently constrained by several techno-economic and infrastructural challenges [15]. The production of green hydrogen remains costly compared to conventional methods that primarily rely on fossil fuels, due to the high investment cost associated with electrolyzers. Furthermore, significant infrastructural developments are required for hydrogen storage (due to its high volume and low density, requiring high-pressure or cryogenic solutions [16]), and distribution to enable its use in residential heating, as previously discussed. While declining renewable energy prices and advancements in electrolyzer technology could make it economically competitive with natural gas prices by 2050 [14], current production remains limited. As of today, 96 % of hydrogen is fossil fuel-derived. Only the remaining 4 % of hydrogen is produced via electrolysis, and only 1 % of that is currently based on renewable energy [17].

Renewable energy technologies such as photovoltaic (PV), solar thermal (ST), and photovoltaic-thermal (PVT) systems are critical for decarbonizing energy systems. PV, in particular, has experienced a 90 % reduction in the global weighted average levelized cost of energy (LCOE) for utility-scale PV plants between 2010 and 2023 [18], driven by improvements in manufacturing and materials. These advancements have enabled remarkable growth in the global market and have made solar energy one of the most affordable electricity sources [19]. By 2021, PV supplied about 3.6% of the world's electricity, with continued growth expected in the coming years [20]. In contrast, ST converts sunlight into heat, offering a sustainable alternative to fossil fuels in heating applications. By 2023, global solar thermal capacity reached 560 GW_{th} (800 million m^2 of collectors), with a 3 % growth from 2022. China leads with evacuated tube collectors, while Europe, the second-largest market, primarily uses flat-plate collectors [21]. Meanwhile, PVT systems combine PV for electricity and ST for heat generation in the same area, resulting in higher overall efficiency and larger energy yields than separate standalone PV or ST systems [22]. While PV cells convert solar irradiation into electricity, the heat they absorb increases their temperature, reducing efficiency (0.2–0.5 %/°C) [23]. PVT's thermal absorber plate captures excess heat from the PV cells with circulating heat transfer fluid (mainly water or air [24]) which is then used for DHW or SH demands. However, high working temperatures lead to greater losses in electrical efficiency, and PV panels have a maximum operation temperature of around 85 °C [25]. Therefore, optimizing the heat-electricity balance remains key. While PVT technology installed capacity is lower than PV and ST technologies, Europe leads the market, which grew 9 % annually (2017–2020), peaking at 13 % in 2021. However, subsidy cuts caused sharp declines in the market (51 % in 2022, 30 % in 2023), reducing its competitiveness compared to more affordable PV systems [21]. They remain, still, particularly valuable when the installation area is limited.

HP systems can be integrated with solar energy technologies (e.g., ST, PVT) to further enhance their efficiency and reduce operational costs. Solar-assisted heat pumps (SAHPs) use solar energy for heat and electricity, increasing renewable energy use and reducing electricity demand [26,27]. SAHPs demonstrate a higher seasonal performance factor but with greater initial costs [27]. They are classified by solar technology (ST/PVT) [27], heat transfer fluid circulation (direct/indirect expansion), and system configuration (parallel/serial/dual source) [28]. Additionally, HPs can be paired with PV systems (PV-HP, typically not classified as SAHPs) to reduce grid electricity use, while PVT-HP systems reduce the HP's workload by utilizing solar energy for both heat and electricity.

When it comes to cooling demand, it is also a significant part of energy needs in Europe, especially in warmer countries like Greece, where it is largely met by electricity-driven systems like air-conditioners (ACs). By contrast, thermally driven cooling systems can directly utilize surplus thermal energy, such as solar thermal heat, thereby reducing reliance on electricity and alleviating peak demand. There is growing interest in absorption refrigeration cycles, especially for large-scale cooling applications. [29]. Direct Absorption Refrigeration (DAR) system [21,24]operates without electricity, has no moving parts, is quiet, is vibration-free, and has a long lifespan [29,30]. Despite these benefits, DAR systems currently exhibit relatively low COP (between 0.12 and 0.35 [30]) and remain limited commercial adoption compared to other cooling technologies. The relevance of DAR systems in modern residential contexts lies primarily in their potential for integration with sustainable heat sources such as solar thermal energy. Their ability to utilize heat makes them particularly suitable for situations where low-grade waste heat or solar thermal energy is readily available [31]. Furthermore, the potential for wider residential adoption is supported by ongoing research and development aimed at overcoming current limitations (e.g., alternative fluids or advanced component designs) [32].

PV modules can contain toxic metals such as lead in solder, the cell metallization layer, or cadmium in thin-film modules, necessitating specialized disposal procedures [1]. If not properly managed, these materials pose severe environmental and human health risks if released into the ecosystem [2]. Proper end-of-life management options include reuse and repair for reuse, recycling, storage, and disposal. Recycling is a preferred option that helps reduce environmental impact and allows for the recovery of valuable materials [1]. PVT systems present even greater recycling challenges due to their integrated design, which complicates material separation and recovery. When examining solar thermal collectors, they are generally considered to have fewer hazardous components compared to PV systems [3]. However, their HTFs, often glycol-based, require careful handling and safe disposal to prevent environmental contamination. On the other hand, heat pumps and air conditioners utilize refrigerants, many of which are potent greenhouse gases with significant environmental implications. Regulations concerning the GWP of refrigerants are evolving (e.g., EU F-Gas Regulation [4]), with increasingly stringent requirements for recovery, handling, and disposal. It is essential to implement proper refrigerant recovery procedures during the decommissioning of these systems [5].

In the existing literature, there are numerous studies focusing on the aforementioned technologies, often comparing them in the context of specific demands such as SH and/or DHW. For instance, Ref. [33] compares heat pumps and gas boilers in terms of energy consumption

across different residential building types demonstrating primary energy savings. Similarly, Ref. [34] examines different configurations of PVT and HP, highlighting improvements in COP and energy efficiency. Additionally, Ref. [35] evaluates PV and PVT systems for combined heat and power provision at a sports center in Bari, Italy, comparing their performances with natural gas-fired system. Similarly, Ref. [36] conducts a related study for urban Mediterranean areas. However, these studies do not offer a comprehensive comparison of technologies that address the simultaneous decarbonization of all residential energy demands – SH, DHW, space cooling (SC), and electricity – within a single, integrated analysis.

Moreover, most studies have primarily concentrated on the energetic performance of these systems, paying limited attention to their economic and environmental dimensions. For example, Ref. [37] provides an energetic analysis of a small absorption chiller but does not explore its economic feasibility or environmental benefits. Ref. [38] compares three solar-assisted heat pump systems using PV panels, flat-plate solar collectors, or a combination of both, concluding that PV-HP combination offers the best energy and economic performance for the specified application. Yet this study lacks an examination of the environmental implications of these systems. Furthermore, some studies focus only one location (or climate). For example, Ref. [36] limits its analysis to warm climates without considering colder regions, while [35,38] focus on only one location. While these studies provide valuable insights into technology performance, a significant gap remains: they do not evaluate all relevant technologies across diverse climates, highlighting how system performance can vary within a single study.

This paper aims to fill this knowledge gap with a unified framework that integrates energy, economic, and environmental assessments to holistically compare different system configurations across diverse climatic conditions. The study evaluates a wide range of technologies, including PV, PVT, ST, air-to-air HP, hydrogen and natural gas boilers, DAR, and air-to-air AC. By proposing and analyzing different combinations of these technologies, the study ensures a systematic exploration of available options for SFHs. Our analysis compares technologies based on efficiency, cost, and environmental impact, offering a more comprehensive understanding of system performance and providing a clearer picture of the trade-offs involved. By examining system performance across three European cities (Athens, Strasbourg, and Helsinki), we offer actionable insights applicable to diverse geographic regions, addressing regional variability in both climate and economic factors.

The structure of this study is organized as follows: Section 2 outlines the heating, cooling, and electricity generation and utilization technologies studied, along with potential integrated system configurations. It also details the mathematical models, key assumptions, and decision criteria, as well as covering the data collection process. Section 3 involves the study results, analyzing and comparing the systems' energy, environmental, and techno-economic performance. Finally, Section 4 concludes the study and discusses future research directions.

2. Methodology

This section first provides a detailed description of the system configurations, outlining the main models developed and key associated equations and assumptions. It then presents the economic models applied to evaluate system performance, along with the economic and environmental parameters used for each configuration. Finally, it details the datasets used in the study.

This study investigates and compares nine different energy system configurations using transient models developed to simulate their performance. Real weather data from selected three cities, with hourly energy demand profiles for SH, DHW, SC, and electricity, as well as economic parameters were incorporated to ensure realistic simulations. The models are designed to meet these key building energy demands, while accounting for interactions between energy generation (e.g., electricity and thermal energy in the case of PVT collectors, electricity for PV, or SC for DAR), thermal storage, and consumption. Each model integrates validated engineering equations and manufacturer data for all components (e.g., PVT, HP, storage tanks, etc.). MATLAB [39] and REFPROP [40] are used for simulations and thermodynamic calculations.

2.1. Energy system configurations

The system configurations investigated in this study are as follows:

- System 1: PVT + HP + AC
- System 2. PV + HP + AC
- System 3. HP + AC
- System 4. Natural gas boiler + AC
- System 5. PV + natural gas boiler + AC
- System 6. ST + natural gas boiler + AC
- System 7. PVT + natural gas boiler + AC
- System 8. Hydrogen boiler + AC
- System 9. PVT + DAR + natural gas boiler

This section begins by introducing the model for the PVT + HP + AC system, as it encompasses most equations relevant to all nine systems. The equations are referenced for other system combinations when they also apply. For systems with different configurations or features, their specific equations are introduced separately.

2.1.1. Systems utilizing a heat pump

The proposed PVT + HP + AC system (System 1), PV + HP + AC system (System 2) and HP + AC system (System 3) are schematically shown in Fig. 1, and described in detail in this section.

2.1.1.1. System 1: PVT + HP + AC. The proposed PVT + HP + AC system consists of PVT collectors, a hot water storage tank, a HP, an auxiliary electric heater, two circulation pumps (account for the pressure drops within the loops), and thermally insulated connection pipes, and air-to-air AC for SC. The PVT collectors generate both electricity and heat from incident solar radiation. The electricity generated is used directly to power household appliances, lighting, the circulation pumps, and the heat pump. Excess electricity is fed into the grid using net metering, which provides compensation through feed-in tariffs. The thermal energy collected by the PVT system is transferred to the hot water storage tank via a heat transfer fluid (HTF). When the HTF reaches a sufficiently high temperature, it flows through the tank's heat exchanger coil, transferring heat to the water in the tank, then it circulates back to the PVT module for reheating. The model implements an iterative solution procedure to resolve the coupled thermal-electrical interactions, ensuring convergence of the calculations. Finally, SC is provided independently by the air-to-air AC unit.

The system uses an indirect parallel configuration, where heat input to the hot water tank is supplied from both the PVT collectors and the heat pump, via separate heat exchangers (HEXs). The hot water tank supplies both DHW and SH demands, which are directly delivered via a circulation system. An auxiliary electric heater is available to boost the tank's output temperature as needed, primarily in winter months.

The PVT collector is modeled as a lumped component, using thermal and electrical efficiency curves, in accordance with the recommendations of EN ISO 9806:2017 [41], a commonly adopted practice in the literature. The instantaneous thermal efficiency of the PVT collector is calculated as follows:

$$\eta_{th} = \frac{\dot{m}_f \bullet c_f \bullet \left(T_{fo} - T_{fi}\right)}{G_i \bullet A} = \eta_0 - a_1 \bullet T_r - a_2 \bullet G_i \bullet {T_r}^2 \quad (1)$$

$$T_r = \frac{T_{fm} - T_a}{G_i} \quad (2)$$

In Eq. (1), $\dot{m}_f$, c_f, G_i, and A represent the mass flow rate of the HTF,

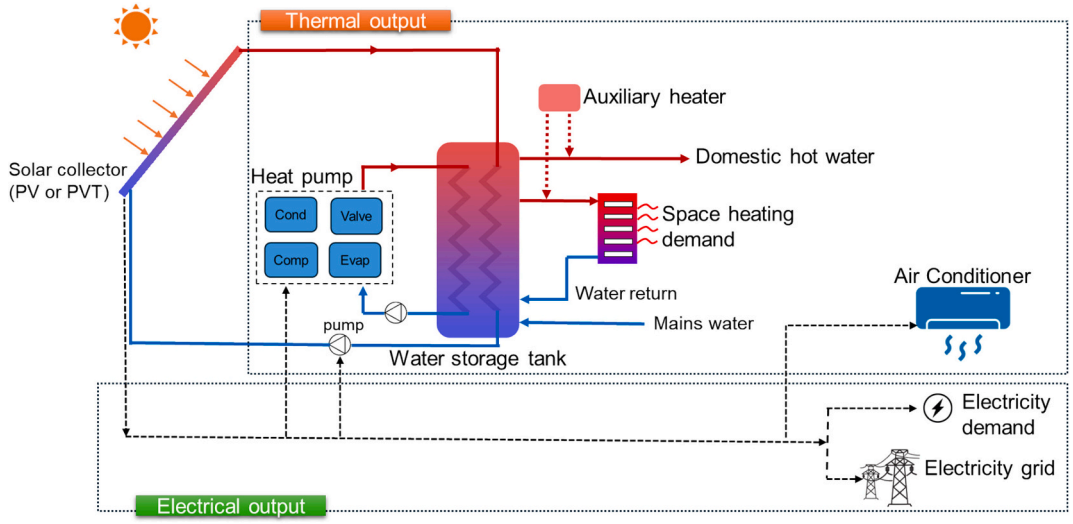

Fig. 1. Schematic diagram of PVT + HP + AC system (System 1). The PVT system produces both thermal energy and electricity generation (System 1). In the PV + HP + AC system configuration (System 2), the PVT system is replaced by the PV system (System 2). The HP-only system (System 3) relies solely on grid electricity.

the specific heat capacity of the HTF, the total solar irradiance, and the collector area, respectively. T_{fo} and T_{fi} are the HTF temperatures at the outlet and inlet of the collector. The coefficients η_0, a_1 and a_2 representing zero-loss efficiency, first-order heat loss coefficient, and second-order heat loss coefficient, respectively. Collector-specific coefficients are provided by the manufacturer and listed in Table 2. They are influenced by factors such as coating quality and absorber design, etc. The reduced temperature(T_r) is calculated as Eq. (2) where T_{fm} (calculated as $(T_{fo} - T_{fi})/2$) and T_a represent, the mean fluid temperature and the ambient temperature, respectively. For a comparison of the model predictions with experimental data based on this formulation, see the validation plot in in Appendix A.5.

The instantaneous electrical efficiency of PVT collectors is calculated using a well-established equation that is commonly used in the literature [42–44]:

$$\eta_{el} = \frac{\dot{E}}{G_i \bullet A} = \eta_{ref} \bullet \left[1 + \beta \bullet \left(T_{mod} - T_{ref}\right)\right] \tag{3}$$

where $\dot{E}$ represents the generated electricity, η_{ref} is reference cell electrical efficiency at the reference temperature T_{ref} at 25 °C, and a solar irradiance of 1000 Wm^{-2}. β is power temperature coefficient, which quantifies the change in efficiency per degree Celsius change in temperature, and T_{mod} is module temperature.

The water storage tank is modeled as a fully mixed tank, assuming uniform temperature distribution within the tank, with the water temperature changing only with time. The total water mass remains constant with steady inflow and outflow, and the water is constant within the operational temperature range [45]. The energy balance equation for the water storage tank is:

$$m_{wt} c_{p,w} \frac{dT_{wt}}{dt} = \dot{Q}_{coil} - \dot{Q}_{SH,cov} - \dot{Q}_{DHW,cov} - \dot{Q}_{losses} \tag{4}$$

The energy equation presented above accounts for $\dot{Q}_{coil}$, which represents the total heat input to the tank in this case it is combination the heat delivered from the PVT collectors, and HP heat output, via their separate immersed HEX. $\dot{Q}_{losses}$ is the heat loss of the water tank to the surroundings. $\dot{Q}_{SH,cov}$, $\dot{Q}_{DHW,cov}$ SH and DHW demands are covered by the water storage tank, respectively. m_{wt}, $c_{p,w}$ are the mass and specific heat capacity of water in the tank, respectively, Finally, T_{wt} is the water temperature in the tank.

The heat delivered to the water tank via the immersed coil heat exchanger, $\dot{Q}_{coil}$ is calculated using the effectiveness-NTU method:

$$\dot{Q}_{coil} = \varepsilon_{hx} \bullet \dot{m}_f \bullet c_p \bullet \left(T_{fo} - T_{fi}\right) \tag{5}$$

Here, ε_{hx} is the heat transfer effectiveness of the HEX coil in the tank. The specific relationship between ε_{hx} and NTU is [46]:

$$\varepsilon_{hx} = 1 - e^{(-NTU)} \tag{6}$$

$$NTU = \frac{A}{\dot{m}_f c_p R_{coil}} \tag{7}$$

The thermal resistance of the coil R_{coil} is calculated by the combined effects of forced convection within the coil, free convection in the tank, and the thermal resistance of the pipe walls. For more information about the resistance of the coil, the reader is directed to Appendix A.1.

Heat losses are considered only for the water storage tank. Losses from other components are assumed negligible due to their shorter retention times and smaller heat transfer fluid volumes compared to the tank. The tank heat losses are calculated using the following equation:

$$\dot{Q}_{losses} = A_{wt} U_{wt} (T_a - T_{WT}) \tag{8}$$

A_{wt} is the tank's external surface area, U_{wt} the overall heat transfer coefficient. It is assumed that a wool insulation layer provides the primary thermal resistance to heat transfer through the tank. The convective thermal resistance, both inside and outside the tank, is considered negligible in comparison. The overall heat transfer coefficient is determined by:

$$U_{wt} = \frac{1}{R_{ins} A_{wt}} \tag{9}$$

The thermal resistance of the insulation for the cylindrical tank is calculated as shown in the following equation:

$$R_{ins} = \frac{ln\left(\frac{r_e}{r_i}\right)}{2\pi k H_i} \tag{10}$$

where r_e and r_i are external and internal radius of the water tank, H_i is internal height of the tank and k is thermal conductivity, which is set to 0.038 W m^{-1} K^{-1} [69].

When solar irradiance is insufficiently low to raise the circulating HTF temperature above the storage tank temperature, the circulation loop is closed to prevent heat loss, and no water circulation occurs. However, it is still necessary to accurately determine panel temperature for calculating electrical efficiency. To achieve this, a new energy bal-

ance is established, accounting for the solar thermal energy absorbed by the panels, convective heat transfer with the surrounding air, and thermal radiation losses. This energy balance is represented by the following equation [47]:

$$m_{\mathrm{col}} c_{p,\mathrm{col}} \frac{dT_{\mathrm{mod}}}{dt} = A_{\mathrm{col}} \left[\alpha G_{\mathrm{i}} \left(1 - \eta_{\mathrm{el,ref}}\right) - h_{\mathrm{conv}} \left(T_{\mathrm{mod}} - T_{\mathrm{a}}\right) - \sigma \varepsilon \left(T^4_{\mathrm{mod}} - T^4_{\mathrm{sky}}\right) \right] \tag{11}$$

where m_{col} $c_{p,\mathrm{col}}$ A_{col} are mass, specific heat capacity, and area of PVT module. The parameters ε, α represent the absorptivity and the emissivity of the PVT module, respectively. h_{conv} is the convective heat transfer coefficient between the PVT module and the surrounding air. σ is Stefan-Boltzmann constant, and T_{sky} representative temperature of the sky (calculated as $0.552 T_{\mathrm{a}}^{0.15}$).

The convective heat transfer is determined by the following equation:

$$h_{\mathrm{conv}} = Nu \frac{\lambda_{\mathrm{air}}}{L_{\mathrm{PV}}} \tag{12}$$

where Nu, λ_{air}, L_{PV} are Nusselt number, thermal conductivity of air, and length of the PVT collector, respectively.

The Nusselt number is determined by the following equation:

$$\mathrm{Nu} = \begin{cases} 0.664 \mathrm{Re}^{0.5} \mathrm{Pr}^{0.3333} & \text{if } \mathrm{Re} \leq 2 \bullet 10^5 \\ 0.036 \mathrm{Re}^{0.8} \mathrm{Pr}^{0.43} - 9400 & \text{if } \mathrm{Re} \geq 2 \bullet 10^5 \end{cases} \tag{13}$$

where Re, and Pr are Reynolds number and Prandtl number, respectively.

When it comes to HP, its performance is modeled using temperature-dependent COP values, which vary with seasonal outdoor and indoor temperature conditions. The model assumes that thermal demand is always satisfied. Its operation is controlled by two main conditions: maintaining the tank temperature above 50 °C and utilizing any excess electricity after meeting the demand for appliances and lighting. The first condition takes priority, so the heat pump operates in two modes: an on-off mode to maintain the tank temperature and a variable heat output mode when excess electricity is available. The following equation summarizes the instantaneous heat output of the HP:

$$\dot{Q}_{\mathrm{HP}} = \begin{cases} \dot{Q}_{\mathrm{max}} & \textit{if } T_{\mathrm{wt}} \leq T_{\mathrm{min}} \\ f\left(P_{\mathrm{exc,app}}\right) & \textit{if } P_{\mathrm{exc,app}} \geq P_{\mathrm{exc,lim}} \&\& T_{\mathrm{max}} \geq T_{\mathrm{WT}} \geq T_{\mathrm{min}} \\ 0 & \textit{if } P_{\mathrm{exc,app}} < P_{\mathrm{exc,lim}} \&\& T_{\mathrm{WT}} \geq T_{\mathrm{min}} \end{cases} \tag{14}$$

$\dot{Q}_{\mathrm{HP}}$, and $\dot{Q}_{\mathrm{max}}$ are the heat output and design (maximum) heat output from the HP, respectively. T_{min} (55 °C) and T_{max} (65 °C) represent minimum and maximum temperature setpoints for HP, respectively. The HP operates at full power when the tank temperature is above T_{min} and is deactivated above T_{max}, even if excess electricity is available. $P_{\mathrm{exc,app}}$ is the excess electrical power remaining from PVT generation after fulfilling the demands of lighting and other appliances. Finally, $P_{\mathrm{exc,lim}}$ is the activation limit for the HP: it is activated if excess power exceeds this threshold. It is set to half the electricity required for the heat pump's minimum part-load operation (the minimum part load is assumed to be half of the design heat output). This strategy is done to optimize solar-sourced electricity. Initially, up to 50 % of electricity is sourced from the grid, as this trade-off is beneficial. Since the HP has a COP greater than 1, utilizing solar energy increases its value. This approach effectively pre-charges the thermal storage tank using a combination of grid electricity and PVT generated electricity, thereby reducing the need for immediate full-grid power later. Activating the HP during high excess PV power saves costs and lowers emissions.

The variable heat output function (denoted as 'f') varies based on the amount of excess electricity, and its mathematical expression for this function is:

$$f\left(P_{\mathrm{exc,app}}\right) = \begin{cases} \dfrac{\dot{Q}_{max}}{2} & \textit{if } P_{\mathrm{exc,app}} < \dfrac{\dot{Q}_{\mathrm{max}}}{2*COP} \\ P_{\mathrm{exc,app}} * COP & \textit{if} P_{\mathrm{exc,app}} \in \left[P_{\mathrm{exc,app}} < \dfrac{\dot{Q}_{\mathrm{max}}}{2*COP}, \dfrac{\dot{Q}_{\mathrm{max}}}{COP} \right] \\ \dot{Q}_{\mathrm{max}} & \textit{if } P_{\mathrm{exc,app}} > \dfrac{\dot{Q}_{\mathrm{max}}}{COP} \end{cases} \tag{15}$$

If $P_{\mathrm{exc,app}}$ is lower than the electricity required for the minimum part load, the HP operates at part load, where the excess electricity supplied by the PVT collector is utilized, and the remaining electricity demand is met by the grid. Conversely, if the excess electricity exceeds the electricity required for the heat pump's full-load operation, the heat pump operates at full load. For intermediate cases, the heat pump's operation is determined by $P_{\mathrm{exc,app}} * COP$.

A validated spatially lumped model [48–50] of a single-stage compressor HP was used to simulate its operation, with fluid properties determined via REFPROP [40] in MATLAB [39]. The model assumes steady-state operation, isenthalpic expansion in the valve, and negligible pressure and heat losses. A rotary vane compressor with R32 as the refrigerant is used in the model, since there is a movement towards lower global warming potential (GWP) refrigerants. R32 has a GWP (on a 100-year timeframe) of 675 kg-$CO_{2,eq}$ per kg refrigerant, whereas widely used R410A has 2088 kg-$CO_{2,eq}$ per kg refrigerant [51]. Performance maps predicting isentropic efficiency based on volume ratio and inlet volumetric flow rate were integrated into the thermodynamic model. The design model was used to obtain optimal heat pump designs for each of the three different locations based on design temperatures aligned with each location's weather characteristics. Compressor efficiency was calculated using fluid properties and ten-coefficient polynomials, assuming 95 % motor efficiency. Off-design performance was adapted to time-varying heat-source conditions, resulting in COP/temperature correlations that serve as inputs for the transient model, and the correlations for each HP can be seen in Fig. 2.

The electricity consumption of the heat pump is calculated using its COP. Furthermore, the electricity consumption of the auxiliary heater,

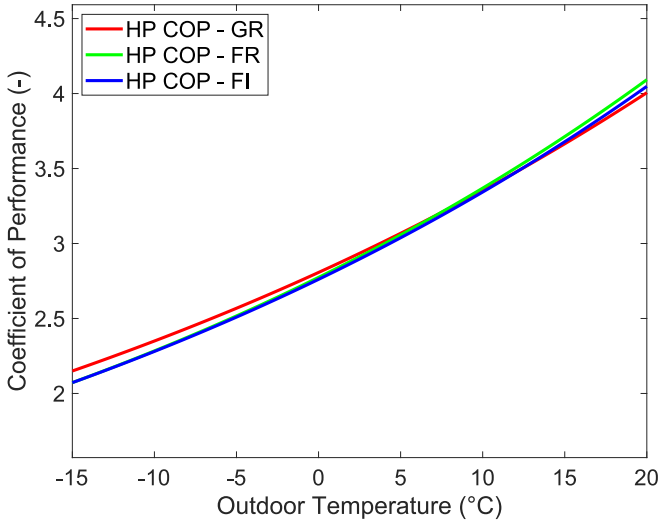

Fig. 2. COP of HP as a function of outdoor air temperature for HPs selected for each city. Minor deviations are observed due to differences in design temperatures specific to each location.

which is considered as part of the HP, is also included in the calculation, see the next equation:

$$P_{\mathrm{HP}} = \frac{\dot{Q}_{\mathrm{HP}}}{COP} + P_{\mathrm{aux}} \tag{16}$$

The auxiliary electrical heater, which is a small extension of the HP system, activates only to boost the tank temperature when the HP is insufficient, which is set to when $T_{\mathrm{WT}} < 50\ ^{\circ}\mathrm{C}$. It operates rarely and its thermal output is regulated by an on-off control and included in HP's overall costs. The COP of the auxiliary heater is assumed to be 1, meaning its electricity consumption equals its heat generation.

Space heating demand is determined by the following equation:

$$\dot{Q}_{\mathrm{dem,SH}} = \dot{m}_{\mathrm{dem,SH}} c_{p,\mathrm{w}} \left(T_{\mathrm{feed,SH}} - T_{\mathrm{in,SH}}\right) \tag{17}$$

The system is designed to continuously meet all heating demands, yet the risk of insufficient tank temperature requires careful analysis, as shown in the following equation:

$$\dot{Q}_{\mathrm{SH,cov}} = \begin{cases} \dot{Q}_{\mathrm{dem,SH}} & \text{if } T_{\mathrm{WT}} \geq T_{\mathrm{feed,SH}} \\ \dot{m}_{\mathrm{dem,SH}} c_{p,\mathrm{w}} \left(T_{\mathrm{WT}} - T_{\mathrm{in,SH}}\right) & \text{if } T_{\mathrm{WT}} > T_{\mathrm{in,SH}} \quad \# \\ 0 & \text{if } T_{\mathrm{WT}} < T_{\mathrm{in,SH}} \end{cases} \tag{18}$$

Full coverage is achieved when the tank water is hotter than space heating feed (set to 50 °C); partial coverage (supplemented by the auxiliary heater) occurs when the tank temperature falls between the required and temperature of water to be heated (set to 30 °C), and the auxiliary heater provides all energy when the tank is at or below the mains temperature.

The DHW demand is determined by the following equation:

$$\dot{Q}_{\mathrm{dem,DHW}} = \dot{m}_{\mathrm{dem,DHW}} c_{p,\mathrm{w}} \left(T_{\mathrm{feed,DHW}} - T_{\mathrm{in,DHW}}\right) \tag{19}$$

$$\dot{Q}_{\mathrm{HW,cov}} = \begin{cases} \dot{Q}_{\mathrm{dem,DHW}} & \text{if } T_{\mathrm{WT}} \geq T_{\mathrm{feed,DHW}} \\ \dot{m}_{\mathrm{dem,DHW}} c_{p,\mathrm{w}} \left(T_{\mathrm{WT}} - T_{\mathrm{in,DHW}}\right) & \text{if } T_{\mathrm{WT}} > T_{\mathrm{in,DHW}} \\ 0 & \text{if } T_{\mathrm{WT}} < T_{\mathrm{in,DHW}} \end{cases} \tag{20}$$

where $T_{\mathrm{in,DHW}}$ is the mains water temperature (set to 10 °C), and temperature for the hot water feed set to 45 °C [52].

To evaluate the performance of AC systems, data from two leading brands, comprising 18 different AC units, were analyzed. This data was obtained from the manufacturers' datasheets. For these evaluations, the indoor air temperature was maintained at 19 °C (wet bulb), meeting standard operating conditions. The outdoor temperature and Energy Efficiency Ratio (EER) relation were examined, as shown in Fig. 3, resulting in the development of a fitting curve that describes this relationship.

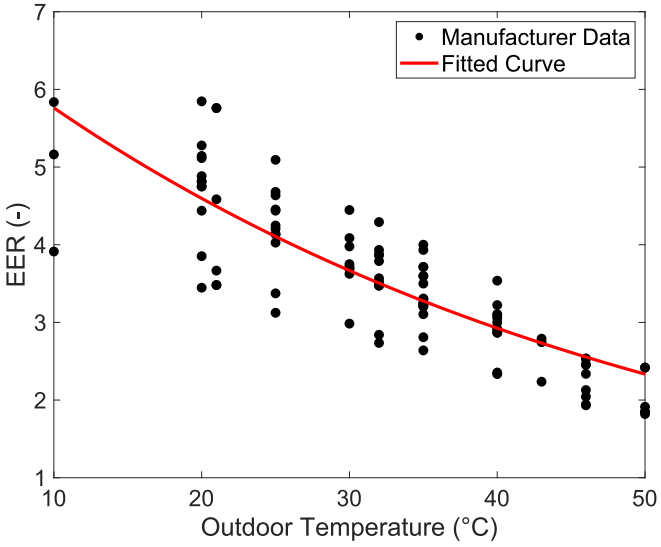

Fig. 3. EER as a function of outdoor air temperature.

The relationship between EER and outdoor temperature is described by:

$$EER = 7.7253e^{(-0.025 \bullet T_{\mathrm{a}})} \tag{21}$$

Finally, the electric power required to run the AC system is given by:

$$P_{\mathrm{AC}} = \frac{\dot{Q}_{\mathrm{dem,SC}}}{EER} \tag{22}$$

2.1.1.2. System 2: PV + HP + AC. The configuration of the PV – HP system is shown in Fig. 1, but in this configuration, there is no thermal energy generation. The electricity generated by the PV panel is directly used to cover the electricity demand of other appliances and/or HP, and any excess electricity is fed into the grid via net-metering. The electricity demand not covered by the PV system is supplied by the electricity grid.

Panel temperatures are determined by Eq. (11), following the same approach applied during periods when the circulation loop in the PVT-HP model is closed. The PV panels are modeled based on their electrical efficiency curve, as described by Eq. (3).

2.1.1.3. System 3: HP + AC. In this configuration, HP covers all SH and DHW, and SC is provided by AC unit. Furthermore, all electricity demand (HP, appliances, and lightning) relies solely on grid electricity, since there are no solar energy sources such as PV or PVT systems. HP is controlled with simple on-off mode depending on the temperature of water in storage tank as follow:

$$\dot{Q}_{\mathrm{HP}} = \begin{cases} \dot{Q}_{\max}, & \text{if } T_{\mathrm{wt}} \leq T_{\min} \\ 0, & \text{if } T_{\mathrm{wt}} > T_{\min} \end{cases} \tag{23}$$

where the electricity consumption of the standalone HP is governed with Eq. (16).

2.1.2. Systems utilizing a boiler

The proposed natural gas boiler + AC system (System 4), PV + natural gas boiler + AC system (System 5), ST + natural gas boiler + AC system (System 6) and PVT + natural gas boiler + AC system (System 7) are schematically shown in Fig. 4 and described in detail in this section.

2.1.2.1. System 4: Natural gas boiler + AC. This configuration uses a natural gas boiler to cover all SH and DHW demands and uses AC for SC demand. All electricity demand is covered by the public electricity grid, as illustrated in Fig. 4. The yearly natural gas consumption can be easily calculated as follows:

$$E_{\mathrm{ng}} = \frac{Q_{\mathrm{dem}}}{\eta_{\mathrm{boiler}}} \tag{24}$$

where E_{ng} is the energy content of the consumed natural gas in kWh Q_{dem} is total heating demand, and η_{boiler} is the efficiency of the natural gas boiler, which is set to 82 % [35].

2.1.2.2. System 5: PV + natural gas boiler + AC. This configuration utilizes PV collectors to generate electricity, and there is no thermal energy generation. The electricity generated by the PV panels is directly utilized to meet the electricity demand of appliances, and any surplus electricity is fed into the grid through net-metering. When the PV system's output is insufficient to meet the electricity demand, the public electricity grid supplies the deficit. Thermal energy demands are

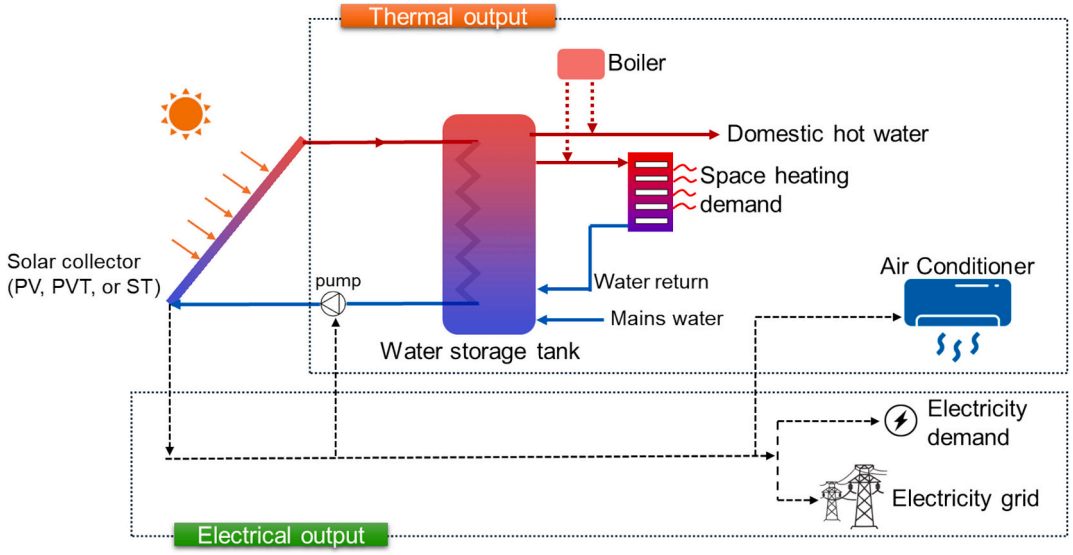

Fig. 4. Schematic diagram of System 4, which represents the natural gas boiler + AC system, System 5, which incorporates a PV system for electricity generation alongside a natural gas boiler and AC, System 6, which uses a ST system for thermal energy generation with a natural gas boiler and AC, and System 7, which combines a PVT system – providing both thermal energy and electricity – with a natural gas boiler and AC.

covered by natural gas boiler, and SC is provided by AC unit.

The electrical performance of the PV modules is modeled using their electrical efficiency curves, as described by Eq. (3), and the module temperatures are determined using Eq. (11), following the same approach as in the PVT-HP model when the circulation loop is closed. The annual energy consumption of the AC unit and natural gas consumption of the boiler are calculated using, respectively.

2.1.2.3. System 6: ST + natural gas boiler + AC. This configuration employs ST collectors to generate thermal energy, which is transferred to a hot water storage tank via a HEX, as described by Eqs. (5)–(7). The thermal energy produced by the ST system is used to meet heating demands, either partially or fully. When the ST system's output is insufficient to meet the thermal load, a natural gas boiler provides the necessary heating. An iterative solution procedure is employed to simultaneously solve the coupled energy balance equations, Eq. (4) for storage tank, Eqs. (1)–(2) the collector fluid, Eq. (17)–(20) for SH and DHW demands. Space cooling is provided by an AC unit. This configuration does not involve electricity generation, therefore, electricity demand is fully supplied by the public electricity grid. The annual energy consumption of the AC unit and natural gas consumption of the boiler are calculated using Eqs. (22) and (24), respectively.

2.1.2.4. System 7: PVT + natural gas boiler + AC. This configuration uses PVT collectors to generate both electricity and thermal energy, as illustrated in Fig. 4. The generated electricity is used to meet the electricity demand, with any excess electricity fed into the grid via net-metering. Generated thermal energy is transferred to a hot water storage tank via an HEX, as described by Eqs. (5)–(7). When the PVT system's thermal output is insufficient, the natural gas boiler supplies the necessary thermal energy.

The electrical and thermal performance of the PVT collectors is modeled using their respective efficiency curves, with Eq. (1)–(2). The water storage tank is modeled based on Eq. (4). The annual energy consumption of the AC unit and natural gas consumption of the boiler are calculated using Eqs. (22) and (24), respectively.

2.1.2.5. System 8: Hydrogen boiler + AC. This configuration follows the same setup as the stand-alone natural gas boiler (System 4) shown in Fig. 4 and uses a hydrogen boiler to meet all SH and DHW demands, while an AC is used for SC demand. All electricity requirements are supplied by the public electricity grid. The yearly hydrogen consumption is calculated based on the following methodology.

The combustion reaction in the boiler is:

$$H_2 + \frac{\varphi}{2}(O_2 + 3.76N_2) \rightarrow H_2O + \frac{(\varphi - 1)}{2}O_2 + \frac{3.76\varphi}{2}N_2 \tag{25}$$

Here, φ represents the excess air ratio, set at 1.13, [53]. 3.76 is the nitrogen-to-oxygen ratio in the air. As a result, the total molar flow rate of the flue gases $\dot{n}_{fg}$ is

$$\dot{n}_{fg} = \dot{n}_{H_2}\left(1 + \frac{\varphi - 1}{2} + \frac{3.76\varphi}{2}\right) \tag{26}$$

In the catalytic boiler, hydrogen reacts at approximately 300 °C. The weighted molar heat capacity of flue gases ($\overline{c_{p,fg}}$) is calculated using mole fractions of each product and their individual heat capacities. Energy losses include sensible heat ($\dot{Q}_{fg,sen}$) and latent heat ($\dot{Q}_{fg,lat}$) from water vapor:

$$\dot{Q}_{fg,sen} = \dot{n}_{fg}\overline{c_{p,fg}}\left(T_{fg} - T_0\right)$$

$$\dot{Q}_{fg,lat} = \dot{n}_{fg}\, x_{H_2O}\, M_{H_2O}\, L_{H_2O} \tag{27}$$

where T_{fg}, T_0 are flue gas temperature and ambient temperature, respectively. x_{H_2O} is the mole fraction of water in the flue gas stream, M_{H_2O} is the molar mass of water, and L_{H_2O} is the latent heat of vaporization. Summing up these two effects give:

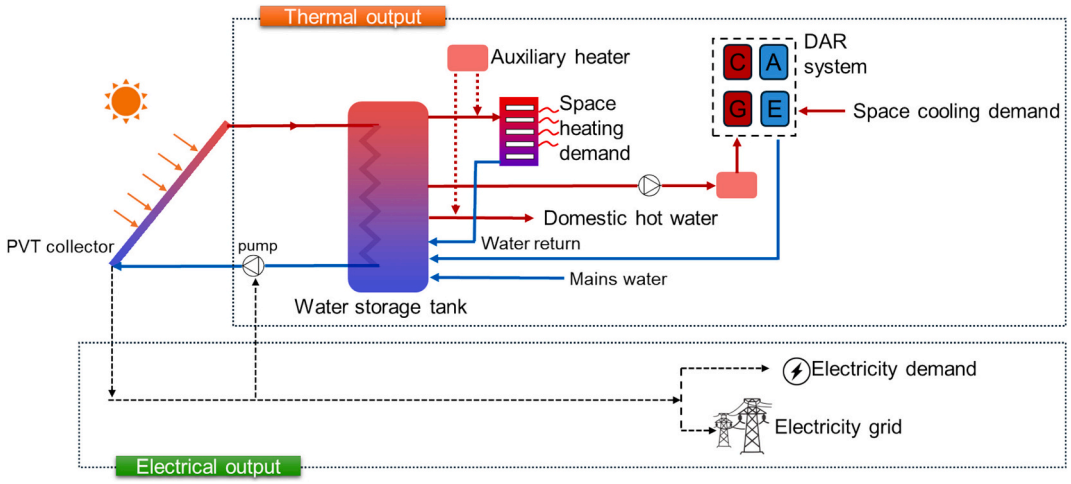

Fig. 5. Schematic diagram of the integrated PVT-DAR System.

$$\dot{Q}_{fg} = \dot{Q}_{fg,sen} + \dot{Q}_{fg,lat} \tag{28}$$

The fuel energy ($\dot{Q}_{fuel}$) required to run the boiler is:

$$\dot{Q}_{fuel} = \dot{Q}_{out} + \dot{Q}_{fg} + \dot{Q}_{loss} \tag{29}$$

where $\dot{Q}_{out}$ is the heat supplied by the boiler, and $\dot{Q}_{loss}$ (1 % $\dot{Q}_{out}$ +$\dot{Q}_{fg}$) is the heat loss from the boiler structure. Condensing boilers reduce losses by condensing water vapor. The required hydrogen mass flow rate ($\dot{m}_{fuel}$) into the boiler is calculated as:

$$\dot{m}_{fuel} = \frac{\dot{Q}_{fuel}}{HV_{fuel}} \tag{30}$$

where HV_{fuel} by the lower heating value of hydrogen.

2.1.2.6. System 9: PVT + DAR + natural gas boiler. The proposed PVT-DAR system, shown in Fig. 5, consists of PVT collectors, a hot water storage tank, an auxiliary heater, circulation pumps (accounts for the pressure drops within the loops, more information see Appendix 2.), insulated connection pipes, and DAR system for SC. The excess heat generated by PVT can then be directed to the DAR system, enabling cooling provision for the building.

The integration of the three subsystems aims to generate electricity to meet partial or total demand, with excess electricity exported to the grid. The extracted thermal energy from PVT collectors is stored in a water tank, which is used to meet SH, DHW, and DAR system heat demands, either fully or partially. Additional heat for SH, HW, and DAR is supplied by an auxiliary water heater when necessary.

For residential and light commercial refrigeration applications, particularly in smaller capacity units, the NH_3-H_2O mixture is widely applied and commercially the most common working fluid pair [54]. This is primarily due to ammonia's low freezing point, the mixture's moderate working pressures, and crucially, its wide operating range without the crystallization risks associated with pairs like H_2O-LiBr [55]. Also, NH_3 has no cumulative effects on the environment with GWP of 0 [56]. A key feature of the analyzed DAR cycle [30] is the use of hydrogen as a non-condensable auxiliary gas (along with a refrigerant and absorbent) to ensure a single pressure, thus replacing the liquid compressor with thermally-driven bubble pump. For detailed process please see Appendix A.6. The hydrogen gas is assumed as a non-condensable ideal gas, particularly in the evaporator section, where its presence facilitates the evaporation of the refrigerant at a lower partial pressure. Also, the total system pressure remains nearly constant, with only minor hydrostatic variations."

The electricity and thermal energy generation of the PVT collectors aligns with the Eqs. (1)–(3). Eqs. (5)–(8), previously explained, are also utilized here for the same purposes. The energy balance for the water storage tank is expressed by Eq. 4, which includes the term $\dot{Q}_{SC}$ to account for the heat supplied to the DAR system, as can be seen in the following equation:

$$m_{wt}c_{p,w}\frac{dT_{wt}}{dt} = \dot{Q}_{coil} - \dot{Q}_{SH,cov} - \dot{Q}_{DHW,cov} - \dot{Q}_{losses} - \dot{Q}_{SC,gen} \tag{31}$$

A validated DAR model is adopted from [57], and is used to determine the required generator thermal power and temperature based on the ambient temperature and cooling demand, as described by Eqs. (32) and (33). The validated model is derived from [57]. The supplied heat must raise the generator's wall temperature to a minimum level in order to initiate the evaporation process for the working fluid. This minimum wall temperature, T_{gen}, is calculated using the following formula [57]:

$$T_{gen} = e(T_{amb})^f \left(\dot{Q}_{gen,exp}\right)^g + h \tag{32}$$

where $\dot{Q}_{gen,exp}$ corresponds to the experimental input heat data, while e,f, g and h are empirical constants that characterize the specific thermal and operational characteristics of the system, T_{amb} and is the ambient temperature in Kelvin.

The heat input required continuous operation of the generator is calculated using the following equation [57]:

$$\dot{Q}_{gen} = N_{DAR}\frac{\left[a(T_{amb})^b\left(\frac{\dot{Q}_{sc,dem}}{N_{DAR}}\right)^c + d\right](T_{AC} + 273.165)(T_{amb} - 5)}{278.16(T_{amb} + T_{AC})} \tag{33}$$

where $\dot{Q}_{gen}$ is the required minimum heat input for all the generators for the cooling system. $\dot{Q}_{sc,dem}$ corresponds to space cooling demand, while

T_{AC} (18 °C) is the desired cooling temperature to be achieved. a,b,c,d are empirical constants. Finally, N_{DAR} is total number of DAR units required to meet the cooling demand. It is important to note that, depending on the space cooling requirements, several DAR units might be required, affecting the total generator required heat input and mass flow ($\dot{m}_{\mathrm{sc,cov}}$) going from the water tank to the cooling system.

A HEX is used in the generator for the heat transfer between the hot water supplied from the water tank and the working fluid inside the DAR unit. A review of DAR systems reveals that generator's heat exchanger design varies widely [31]. While numerous studies have investigated the performance and thermodynamic parameters of DAR systems, there is limited experimental data on heat transfer properties for modeling generators with heated water. To address this, data from conventional absorption chillers is used as a reference to estimate practical heat transfer values for the generator, even though they are not identical to DAR units. Parameters from [37] were used as references for the numerical calculations.

The heat delivered to the DAR unit is calculated using the effectiveness-NTU method, as described in Eqs. (6)–(7). Since the design temperatures are unknown, the individual exchanger minimum approach temperature (EMAT) method is used for estimation. This method assumes a 5 °C minimum temperature difference between the hot outlet stream of HEX and the generator temperature (T_{gen}). This assumption ensures sufficient heat transfer and is based on recommendations for refrigerants [58]. While this approach may introduce errors in practical applications, as noted in [59], it is considered sufficient for an initial estimate.

The effectiveness value is then estimated using experimental data from [37] for an absorption chiller with a 4.5 kW cooling capacity. The parameters used include; UA of 1423 W °K^{-1}, a mass flow rate ($\dot{m}_{\mathrm{sc,cov}}$) of 0.25 kg s^{-1}, and heated liquid water at 90 °C as the heating fluid. Although the study used LiBr/H_2O as the working pair, the estimated effectiveness serves as a reference for evaluating the thermodynamic performance of the PVT-DAR system. The main goal of incorporating experimental heat transfer properties is to improve the accuracy of system requirements and develop a more realistic model.

Once the inlet and outlet temperatures are determined, the mass flow needed for the DAR generators can be calculated using the following equation:

$$\dot{m}_{\mathrm{sc,cov}} = \frac{\dot{Q}_{\mathrm{gen}}}{c_{p,\mathrm{w}}\left(T_{\mathrm{in,hot}} - T_{\mathrm{out,hot}}\right)} \tag{34}$$

The additional heat required for the DAR unit, supplied by the auxiliary heater, is calculated as follows:

$$\dot{Q}_{\mathrm{gen}} = \dot{m}_{\mathrm{sc,cov}} c_{p,\mathrm{w}}\left(T_{\mathrm{in,hot}} - T_{\mathrm{wt}}\right) \tag{35}$$

where mass flow refers to the amount required for all the generators in the DAR system.

2.2. Economic and environmental variables

The annual operating cost savings (C_{s}) are defined as the difference compared to the current annual costs to meet all energy demands using System 4 (natural gas boiler + AC). Below, Eq. 36, we provide a general equation for C_{s}, while the system-specific equations can be found in Appendix A.3.

$$C_s = C_{\mathrm{O\&M,boiler}} - C_{\mathrm{O\&M}} + (E_{\mathrm{cov}} - E_{\mathrm{extra}})c_{\mathrm{e}} + E_{\mathrm{exc}}s_{\mathrm{e}} + \frac{(Q_{\mathrm{HW,cov}} + Q_{\mathrm{SH,cov}})c_{\mathrm{ng}}}{\eta_{\mathrm{boiler}}} \tag{36}$$

where $C_{\mathrm{O\&M,boiler}}$, $C_{\mathrm{O\&M}}$ are operation and maintenance costs for System 4 and considered system combination, respectively. E_{cov} is the electricity demand covered for all systems (solar-sourced electricity from PV or PVT collectors, if applicable), while E_{extra} is additional electricity demand (e.g., from HP) that is not covered by solar-sourced electricity, even if present. E_{exc} is the electricity sold to the grid, and c_{e}, s_{e}, c_{ng} are cost, and selling price of electricity, and cost of natural gas, respectively. $Q_{\mathrm{DHW,cov}}$, $Q_{\mathrm{SH,cov}}$ represent DHW, and SH demand covered by system (which can be fully covered by system such as PVT-HP or PV- HP, while in others, such as PVT-NGB, only a portion may be covered). It is important to remember that; PV systems generate only electricity, ST systems generate only thermal energy, PVT systems generate both electricity and thermal energy. Thus, the respective variables in the equation (e.g. E_{cov}) are adjusted accordingly based on the system type [27,35].

The net present value (*NPV*), a method for evaluating the value of an investment, is defined as the sum of all the cash flow over the investment's lifetime, discounted to the present value. It was calculated using the following equation [35]:

$$NPV = -I_o + \frac{C_s}{(d - i_f)}\left[1 - \left(\frac{1 + i_f}{1 + d}\right)\right] \tag{37}$$

where I_{o} is an initial investment, including all system components, and i_f, d are the inflation rate and discount rate, respectively.

The Internal Rate of Return (IRR) is the discount rate at which the NPV of the investment equals zero, providing insight into the project's profitability threshold, and allows for comparison with alternative investment opportunities or required rates of return.

The payback time (*PBT*) determines the time required to recover the initial investment costs and is calculated using the following equation [35]:

$$PBT = \frac{ln\left(\frac{I_o(i_f - d)}{C_s} + 1\right)}{ln\left(\frac{1 + i_f}{1 + d}\right)} \tag{38}$$

The levelized cost of energy in electricity equivalents ($LCOE_{\mathrm{eq,el}}$) evaluates the total costs associated with both the actual electricity output and the equivalent electricity derived from the thermal energy output. It was calculated using the following equation [27]:

$$LCOE_{\mathrm{eq,el}} = \frac{I_o + \sum_{i=1}^{n} C_{\mathrm{prod}}\left(1 + i_f\right)^{i-1}(1 + d)^{-i}}{\sum_{i=1}^{n}(Q_{\mathrm{el}} + Q_{\mathrm{th}}\eta_{\mathrm{th}})(1 + d)^{-i}} \tag{39}$$

Here, C_{prod} is the yearly cost is related to energy production, and Q_{el}, Q_{th} are the net annual production of electricity and heat, respectively. The thermal output is assumed equivalent to the electricity that could have been produced from that heat in a natural gas power plant, with η_{th} the typical efficiency of a modern natural gas power plant, from thermal to electrical.

$LCOE_{\mathrm{eq,el}}$ is used in this study to compare the profitability of different systems, as it accounts for both thermal and electrical generation. For example, SAHP or PV-HP systems produce both thermal and electrical energy, while the standalone HP or boiler system only provides thermal energy. To ensure a fair comparison, all energy consumed by the household, including electricity for appliances, is considered for all systems.

The annual CO_2 emission reduction (*ER*) of the proposed systems is calculated based on the difference in emissions between the proposed

system and the reference system (System 4: Natural gas boiler + AC) as follows [35]:

$$ER = (E_{cov}(i) + E_{exc}(i)) \bullet C_{int}(i) + \frac{(Q_{HW,cov} + Q_{SH,cov})}{\eta_{boiler}} f_{ng} \quad (40)$$

$E_{cov}(i), E_{exc}(i)$ are the electricity covered by PV/PVT collectors, and excess electricity exported to the grid, respectively, at time step *i*. $C_{int}(i)$ is the carbon intensity of the grid electricity at time step *i*, and f_{ng} is the CO_2 emission factor of natural gas. Thus, the emission reduction considers only the operational CO_2 emissions of the proposed system combinations.

The environmental penalty cost savings (*EPCS*) [35,60] represents the financial savings of reduced CO_2 emissions in the proposed systems and is calculated as follows:

$$EPCS = \frac{ER_{tot} C_{CO2}}{(d - i_f)} \left[1 - \left(\frac{1 + i_f}{1 + d}\right)\right] \quad (41)$$

where C_{CO2} is the current unit cost of CO_2 emissions, based EU Emission Trading System (ETS) [61]. For the residential sector, where future carbon pricing is expected [62]. These values indicate the long-term potential of low carbon systems.

2.3. Data collection

Here, you can find an overview of the data sources used in this study. First, we present the selected case study locations and their climate classifications. Next, we describe the required weather data, thermal and electricity demand profiles, and the carbon intensity of grid electricity. Finally, we detail the economic and environmental variables essential for evaluating system performance.

2.3.1. Location selection

Helsinki, Strasbourg, and Athens, which have been chosen to represent cold, mild, and warm climates, respectively, in accordance with the BS EN 14825 standard [63]. These cities were chosen to cover the range of climate zones across Europe, enabling a comprehensive analysis of heating and cooling technologies under different climate conditions (See Fig. 6).

Fig. 6. Europe map with the 3 selected cities.

2.3.2. Input data for weather, energy demand, and emissions

The model requires hourly data on temperature, irradiation, and wind speed, sourced from PVGIS-SARAH3 [64] for selected cities for the year 2022. The tool provided a 2-m air temperature, global irradiance, and 10-m wind speed, and the most significant are presented in Fig. 7.

The normalized demand profiles of SFH for SH and DHW were sourced from the When2Heat Heating Profiles database [65], which provides country-level (NUTS0) hourly residential demand profiles, while data for SC was obtained from Hotmaps project [66], offering regional-level (NUTS2) data. These profiles provide hourly data, expressed in normalized values, where the sum of all hourly values for the given demand over the year equals one. Total annual demands for SH, DHW, and SC were derived from Hotmaps project, and hourly thermal demand, in Watts, was calculated by multiplying normalized profiles by total annual energy demand.

Normalized SH and DHW profiles were taken directly from When2Heat 2022, while SC profiles were adapted using ambient temperature correlations, as stated in the Hotmaps main document [66]. SC demand, influenced by the hour of the day and outside temperature, was used to create yearlong demand profiles for NUTS2 regions, including Uusimaa (Helsinki), Grand Est (Strasbourg), and Central Greece (substituting for Athens region due to data unavailability, assuming no effect on the results as the demand is normalized). Fig. 8 presents the hourly thermal energy demand, showing the variation in heating and cooling needs throughout the year for Helsinki, Strasbourg, and Athens.

To analyze the electricity demand for SFHs (excluding electricity use for heating and cooling), the total annual electricity demand and the normalized electricity load profile were used. Annual consumption data were obtained from the Odyssee-Mure database [67] assuming SFHs consume the same as average dwellings. The hourly normalized electricity load profile for selected countries in 2022 was obtained from the ENTSO-E Transparency Platform. [68], with results shown in Fig. 9.

Fig. 10 shows a comparison of hourly carbon emissions (gCO_2-eq/kWh) for grid electricity, using data from Electricity Maps [69]. In this study, we used 2023 hourly grid emission factors, specific to each country, which are based on a Life Cycle Assessment (LCA) approach. Electricity Maps' methodology [70] accounts for the full life cycle of electricity generation—including fuel extraction, plant construction and dismantlement, direct operations, and end-of-life—using emission factors primarily sourced from the IPCC (2014) Fifth Assessment Report [71] with flow-tracing algorithms to track the origin and production mix of electricity in each zone [70].

The calculated thermal energy demands, presented in kWh/m^2 per year, account for the dwelling area. To derive an overall value, an average dwelling size of 93.1 m^2 (derived from SFH sizes data [66] for Finland, France, and Greece) was used. Using the mean area rather than country-specific house sizes ensures a fair comparison of the technology's performance, independent of variations in house size.

Every building has a defined total roof area, and only a portion of this surface is technically and practically usable for solar collector installation due to several limiting factors. These include roof orientation and slope, which influence solar exposure and electricity generation; shading from near buildings, and trees; and permanent rooftop obstacles such as chimneys [72]. To account for these limitations, studies commonly apply a rooftop utilization factor. Estimating this ratio requires detailed spatial modeling using high-resolution datasets and advanced Geographic Information System (GIS) techniques [73]. These factors vary widely based on building type, urban morphology, and regional characteristics (between 40 % and 70 % depending on the specific context and study methodology [72,74–77]). In this study, a 40 % rooftop utilization factor was applied to account for typical constraints and provide a realistic estimate of available roof area for solar installations.

To convert the rooftop area into usable space for PV/PVT/ST collectors, an average rooftop utilization factor [75] (u_r) was applied. The total available area ($A_{available}$) for the collectors is calculated as:

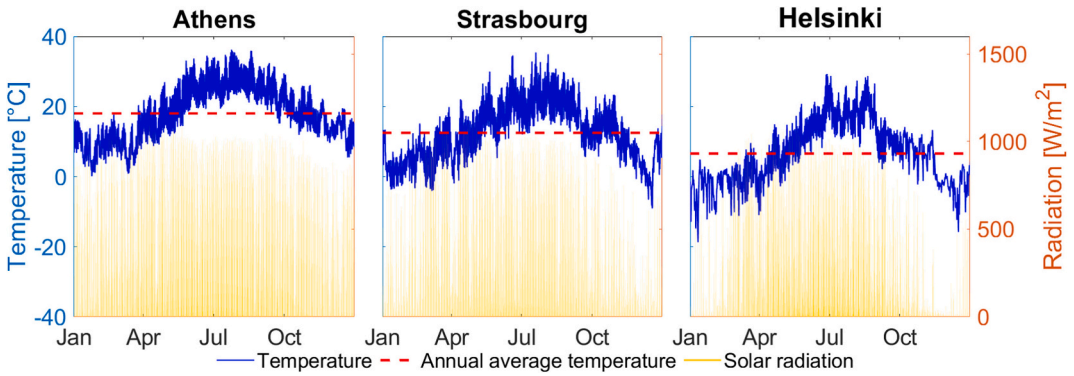

Fig. 7. Relevant weather properties for the three case study locations.

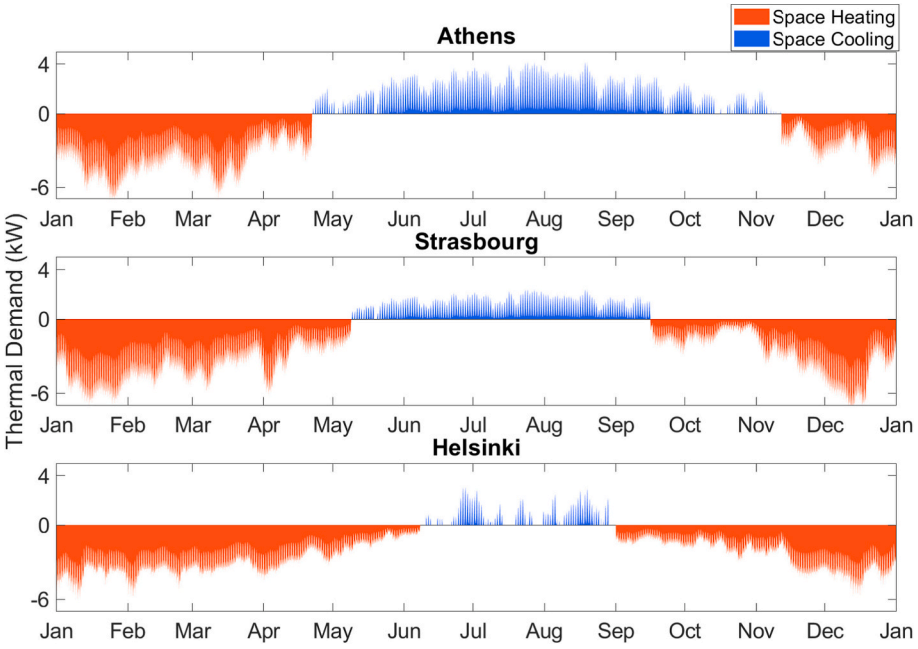

Fig. 8. Thermal load profiles of the SFH for the three case study locations. Negative values represent heating and positive values represent cooling.

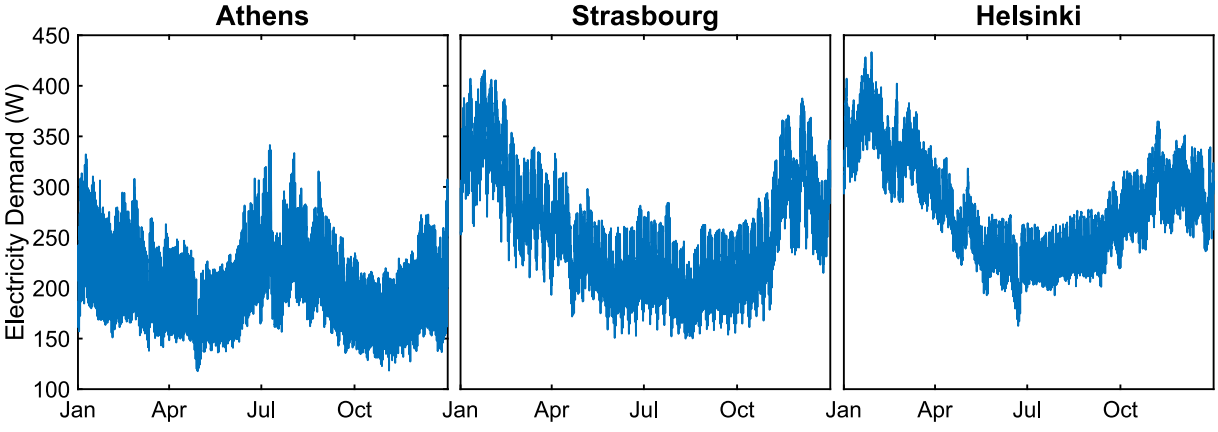

Fig. 9. Hourly electricity demand in the three selected cities.

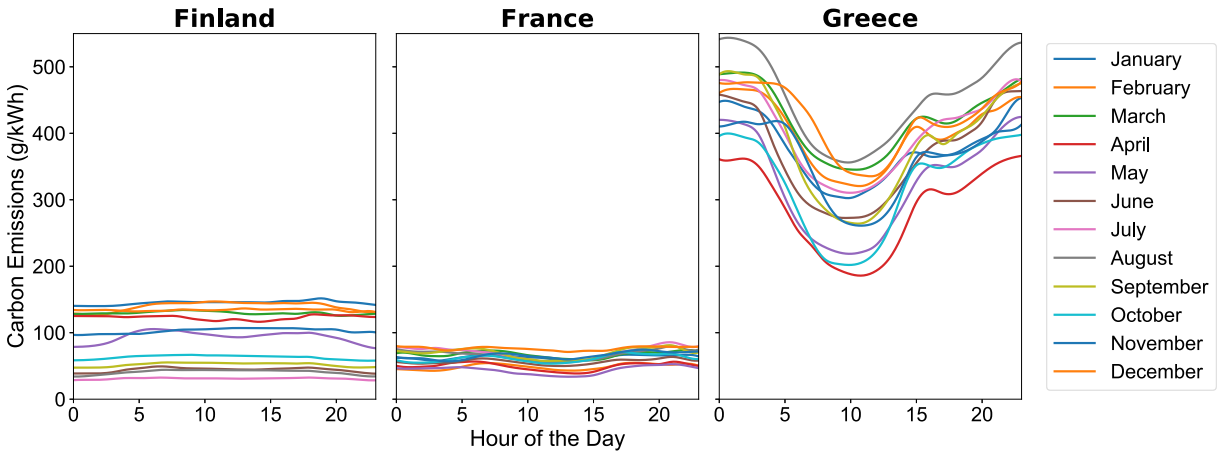

Fig. 10. Hourly carbon intensity of grid electricity.

Table 1
Building specifications of the analyzed SFH.

Specification	Value	Unit
Floor area	93.1	m^2
Roof area	82.4	m^2
Rooftop utilization factor	0.400	Ratio
Available area for PV/PVT/ST	32.9	m^2

Table 2
Main technical parameter of PVT, PV, and ST collectors.

Parameter	Value	Unit
PVT collector	Ecomesh [93]	
Area per collector	1.55	m^2
Absorber-exchanger type	Flat-box	–
Cell type	Polycarbonate	–
Nominal power	260	W_p
Electrical eff. (ref)	15.98	%
Temp. coef. (β)	0.0047	K^{-1}
Thermal eff. (ref)	51	%
1st-order heat loss coefficient	4.93	$W\,m^{-2}\,K^{-1}$
2nd-order heat loss coefficient	0.04	$W\,m^{-2}\,K^{-1}$
PV module	UL-355-120355Wp [94]	
Area per collector	2.01	m^2
Cell type	Poly-crystalline silicon	–
Nominal power	355	W_p
Reference electrical efficiency	17.7	$W\,m^{-2}\,K^{-1}$
Temperature coefficient	−0.36	$W\,m^{-2}\,K^{-1}$
ST collector	Bosch Sonnenkollektor SO4000 TFV-FCC220-2 V [95]	
Area per collector	3.09	m^2
Collector type	Flat plate cov.	–
Intercept thermal efficiency	70.5	%
1st-order heat loss coefficient	3.78	$W\,m^{-2}\,K^{-1}$
2nd-order heat loss coefficient	0.011	$W\,m^{-2}\,K^{-1}$

$$A_{available} = u_r A_r \tag{41}$$

The rooftop area is determined from the constructed floor area(A_f), average number of floors (F), and average roof slope (ν, set to 34°), as follows:

$$A_r = A_f \frac{1+b}{F\cos(\nu)} \tag{42}$$

Table 3
Investment and maintenance costs for components in the analyzed systems.

System	Component	Value	Unit	Reference
PVT System	PVT collector	1.9	€/W_P	[96]
	Expansion Vessel	140	€/set	[45]
	Pipes	11	€m	[45]
	HTF	3.3	€/L	[45]
	Mounting	59	€/collector	[45]
	Installation	40	€/m^2	[35]
	$C_{O\&M}$	0.01 C_0	€/year	[97]
	Controller	110	€	[45]
	Inverter	0.2	€/W_P year	[98]
PV System	PV system	0.85	€/ W_P	[35]
	$C_{O\&M}$	0.015	€/W_P year	[35]
ST System	ST collector	502	€/collector	[99]
	Mounting	56	€/collector	[45]
	Installation	29	€/collector	[45]
	$C_{O\&M}$	0.01 C_0	€/year	[35]
HP System	C_0	4870–5340	€	[50]
	Installation	2530	€	[50]
	$C_{O\&M}$	115	€/year	[50]
Natural gas Boiler	C_0	1730	€	
	Installation	2630	€	
	$C_{O\&M}$	115	€/year	[50]
Water Storage Tank	Tank	1500		[97]
Air Conditioner	C_0	1200	€	
	Installation	500	€	
	$C_{O\&M}$	0.01 C_0	€/year	
DAR system	C_0	600	€/unit	

Table 4
Economic variables.

Parameter	Finland	France	Greece	Units
Electricity purchase price	0.17	0.22	0.28	€/kWh
Electricity selling price	0.09	0.02	0.07	€/kWh
Natural gas price	0.07	0.08	0.07	€/kWh
Hydrogen prices	6.40	6.80	7.00	€/kg
Interannual inflation rate	0.005	0.027	0.03	rate
Discount rate		0.041		rate
Pound to euro conversion		1.17		rate
Emission factor of natural gas		0.200		$kgCO_2$/kWh
Cost of unit CO_2 emission		0.08		€/$kgCO_2$

where b represents an additional factor to account for stairways, corridors, and similar areas, set to 10 %.

House specifications are provided in Table 1. No additional house-specific data is required by the model, as the demand profiles already incorporate heat losses to the environment, eliminating the need to account for insulation properties.

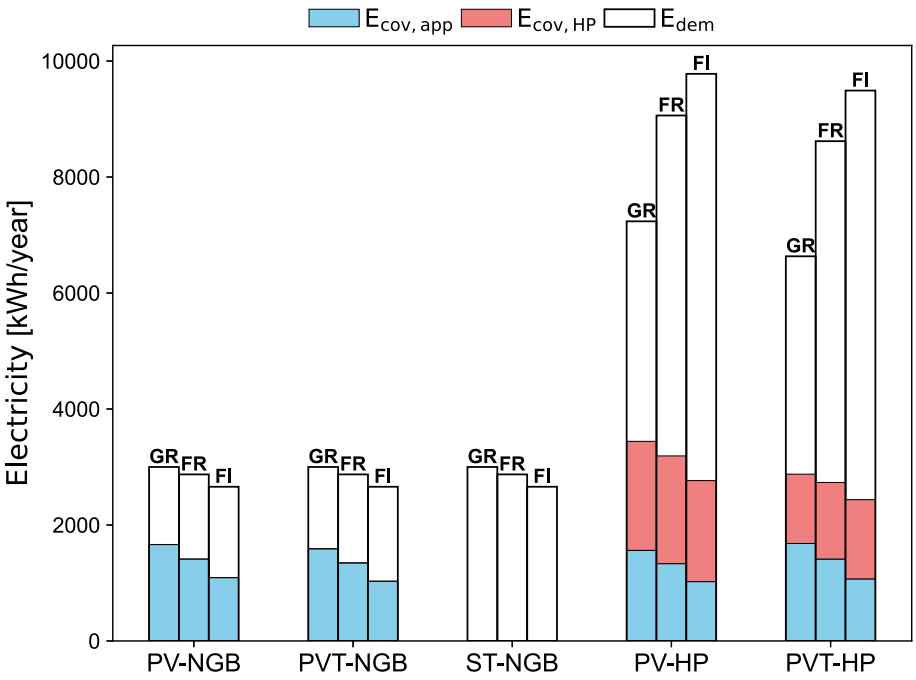

Fig. 11. Annual electricity demand and coverage (from PV or PVT) for different system configurations in the investigated cities. The figure presents the yearly electricity demand (E_{dem}), and solar-sourced electricity contributions covering the heat pump ($E_{cov,HP}$) and household appliances ($E_{cov, app}$). The white portions of the bars indicate the share of electricity supplied by the grid. The numerical data for these results is available in Appendix A.7.

2.3.3. *Economic and environmental variables*

The models require both economic and environmental data as input variables. In Table 2, main technical parameters of PVT, PV, and ST collectors are summarized. System-specific values, such as C_0 and $C_{O\&M}$, are presented in Table 3, assuming that hydrogen boilers cost no more than natural gas boilers [78]. Additional costs such as pumps and pipes are given in Appendix A.4. Natural gas, electricity prices (both buying and selling), currency conversion rates, inflation and discount rates, and emission factor for natural gas are common to all systems but vary by country. These parameters are outlined in Table 4 [79–90]. Typically, values are reported annually, and the most recent data available are used in this study. It is important to note that hydrogen is not yet widely established for residential heating, so we consider using directly connected lowest-cost renewable energy share technology for a given country [91] accounting for distribution and other costs, assume a price increase of 25 % for each [92].

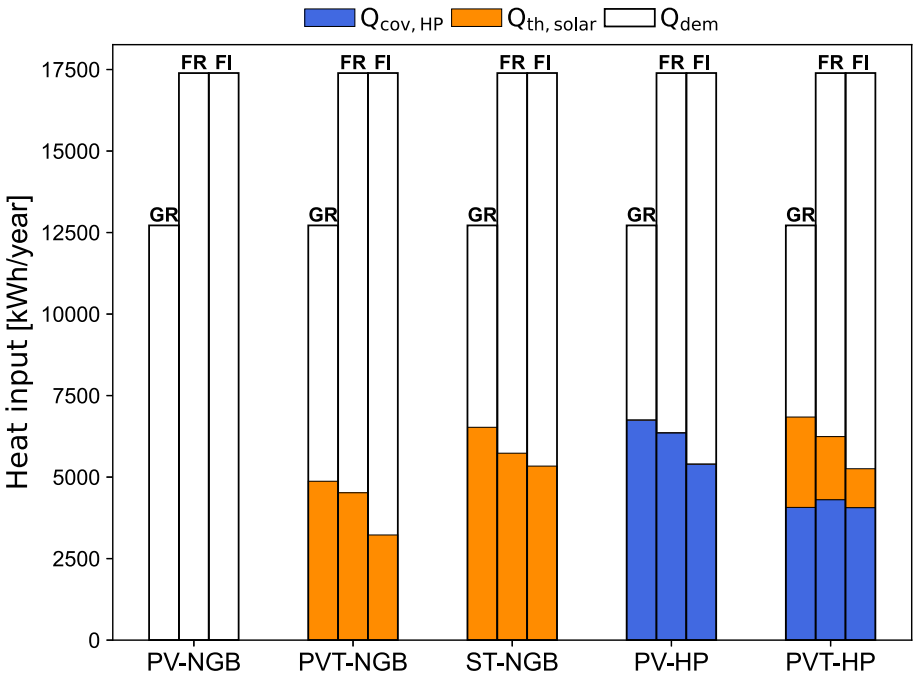

Fig. 12. Annual heat demand and coverage (from PVT or ST) for different system configurations in selected cities. The figure presents the yearly heat demand (Q_{dem}), heat input to the tank via direct solar thermal energy ($Q_{th,solar}$), and solar-sourced electricity used by the heat pump ($Q_{cov,HP}$). The numerical data for these results is available in Appendix A.7.

3. Results and discussion

In this section, we present a performance comparison of various energy system configurations, focusing on electricity and heat coverage, environmental impact, and economic outcomes. We also incorporate sensitivity analyses of varying energy prices to determine the most cost-effective system for each city.

3.1. Performance comparison of different energy systems

Fig. 11 shows the annual results for electricity demand and coverage for analyzed cities. The variation in electricity demand is driven by location-specific load profiles, which include only appliances and lighting. In the MATLAB model, additional electricity demand is calculated and included for SC when the system combination includes an AC. Similarly, electricity demand for SH and DHW is included if the system configuration includes a HP, leading to higher overall electricity demand for these systems. On the other hand, PV-NGB, PVT-NGB, and ST-NGB systems exhibit lower electricity demands for each city, as SH and DHW are provided by boiler or solar sources (PVT or ST depending on the system configuration).

The PV-HP combination achieves electricity coverage rates of 48.0 % in Athens, 35.0 % in Strasbourg, and 28.0 % in Helsinki. This result indicates that with the integration of appropriate battery storage solutions, electricity consumption could be managed more efficiently, leading to cost reductions. The PVT-HP combination achieves the highest electricity coverage among the analyzed systems: 53.1 % in Athens, 39.5 % in Strasbourg, and 31.7 % in Helsinki. This is due to the thermal energy produced by PVT modules, which reduces the HP load and, consequently, electricity consumption. For the COP values of HPs along the year, the reader is referred to Appendix A.7.

For the PV-NGB system (PV + natural gas boiler + AC), the yearly electrical coverage is highest in Athens at 54.7 %, followed by Strasbourg at 50.8 % and Helsinki at 41.1 %, as expected. The PVT-NGB system exhibits slightly lower but comparable electricity coverage rates: 53.0 % in Athens, 49.3 % in Strasbourg, and 39.5 % in Helsinki. These values align with expectations, as the additional thermal energy production of PVT systems slightly reduces their electrical output compared to PV systems.

Fig. 12 demonstrates the heat demand and its breakdown for the same system combinations across analyzed locations. For the ST-NGB system (ST + natural gas boiler + AC), Athens shows a heating coverage of 51.8 %, with contributions of 91.7 % for DHW and 44.8 % for SH. In Strasbourg, the heating coverage decreases slightly to 33.5 %, with DHW and SH contributions of 82.1 % and 27.0 %, respectively. In Helsinki, the corresponding values are 31.6 % for total heating coverage, 71.6 % for DHW, and 25.7 % for SH.

For the PVT-NGB system (PVT + natural gas boiler + AC), the heating coverage in Athens is 38.8 %, with DHW and SH contributing 88.5 % and 30.2 %, respectively. Strasbourg and Helsinki exhibit similar trends but with lower overall heating coverage: 24.0 % in Strasbourg and 19.3 % in Helsinki. In Strasbourg, the DHW contribution decreases to 76.9 %, while SH accounts for 17.0 %. In Helsinki, the respective contributions are further reduced to 62.7 % for DHW and 13.2 % for SH.

3.2. Environmental analysis and comparison

Emission reductions (ER), calculated as the annual difference in emissions between each proposed system and the reference system (System 4: Natural Gas Boiler + AC), are significantly higher in Athens than in Strasbourg or Helsinki when integrating PV and PVT systems. This disparity arises due to the greater carbon intensity of grid electricity

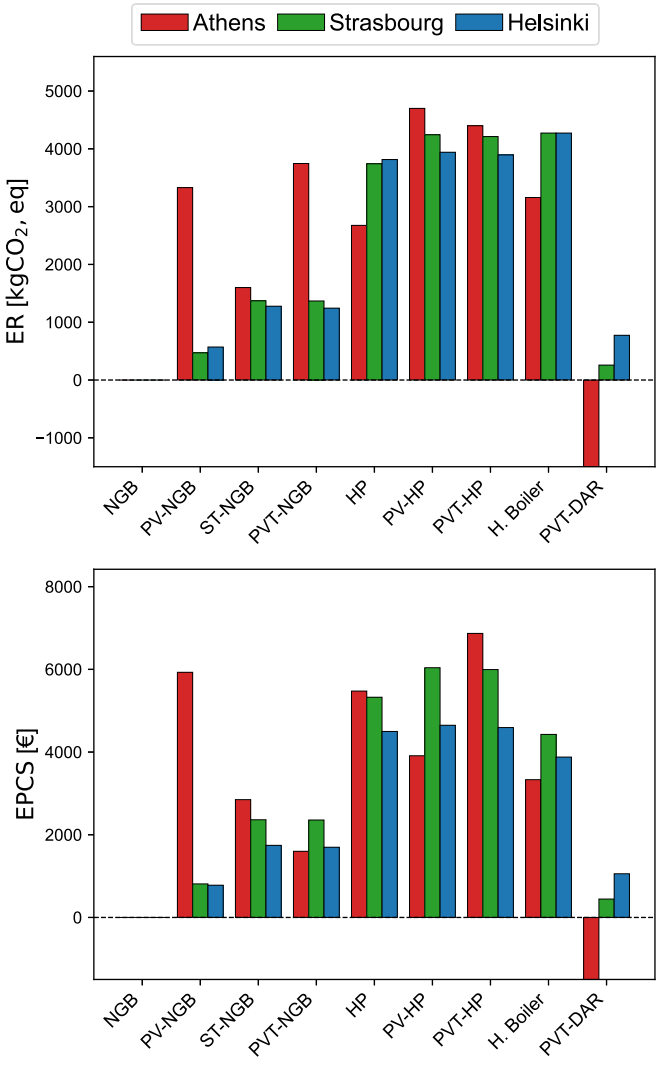

Fig. 13. ER and EPCS for various system combinations in selected cities. ER (−13,200 €/year) and EPCS (− 24,100 €) values for Athens PVT-DAR are not fully displayed to show other values clearly.

in Athens, which was consistently 2 to 5 times higher than in Strasbourg or Helsinki, as illustrated in Fig. 10. This regional variation underscores the importance of considering local grid carbon intensity when evaluating the environmental impact of renewable energy systems.

Similarly, HPs show lower ER values in Athens for the same reason, as their environmental benefits are directly influenced by the carbon intensity of the grid electricity they consume. In contrast, the PV-HP combination demonstrated the highest emission reduction in Athens, achieving approximately 4700 kg $CO_{2,eq}$/year, followed closely by the PVT-HP system, which achieved a slightly lower reduction of about 4400 kg $CO_{2,eq}$/year. In contrast, both systems exhibited lower emission reductions in Strasbourg and Helsinki, achieving approximately 4200 kg $CO_{2,eq}$/year and 3900 kg $CO_{2,eq}$/year, respectively.

Notably, the hydrogen boiler fueled by green hydrogen achieved the highest emission reduction in Strasbourg and Helsinki, reaching approximately 4270 kg $CO_{2,eq}$/year. This result highlights the potential of green hydrogen as a zero-emission heating solution, particularly in regions with high heating demands.

The emissions penalty cost savings (EPCS) quantifies the economic advantages of low-carbon technologies under regulatory frameworks

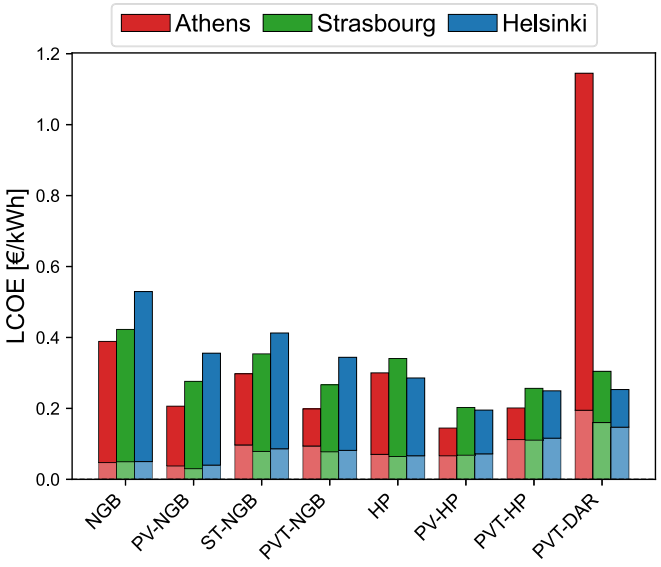

Fig. 14. $LCOE_{eq,el}$ with capital costs (lower segments) and operational costs (upper segments) for various system combinations in selected cities.

such as emission trading systems. As shown in Fig. 13, systems with higher emission reductions, such as the PV-HP and PVT-HP combinations in Athens, achieve greater cost savings through reduced emissions penalties. With many countries planning to increase energy costs tied to carbon emissions, the adoption of low-carbon technologies is becoming increasingly economically attractive.

Annual reduction in CO_2 emissions was achievable for all systems and all cities, except for the PVT-DAR system in Athens, which increased emissions. This stems from Athens' significantly high cooling demand, where the DAR generator relies on a natural gas-powered heater to generate space cooling. This outweighed the CO_2 reductions from reduced grid electricity consumption and partial SH and DHW coverage by PVT system. This highlights the importance of considering location-specific factors, such as climate and energy demand, when evaluating system performance.

3.3. Economic analysis and comparison

Fig. 14 shows the $LCOE_{eq,el}$ with capital costs (lower segments) and operational costs (upper segments) for various analyzed systems across Athens, Strasbourg, and Helsinki. The results indicate that systems incorporating solar technologies, such as PV and PVT systems, generally exhibit lower $LCOE_{eq,el}$ compared to the same system combination without solar technology. Their $LCOE_{eq,el}$ values are 0.1–0.2 euro/kWh lower than those of systems without solar technology, since these systems effectively meet a substantial portion of heating/electricity demand while minimizing operating costs. To give a more detailed picture, stand-alone natural gas boiler systems show relatively low capital costs but high operational costs (0.34 €/kWh in Athens, 0.473 €/kWh in Helsinki) due to fuel expenses. In contrast, heat pump systems (HP, PV-HP, PVT-HP) demonstrate higher capital costs but significantly lower operational costs, particularly when combined with solar technologies (See Fig. 15).

The PV-HP system consistently achieves the lowest values across all cities, ranging from 0.145 €/kWh in Athens to 0.203 €/kWh in Strasbourg. This system's competitiveness results from an optimal balance: moderate capital costs (0.066–0.072 €/kWh) combined with very low

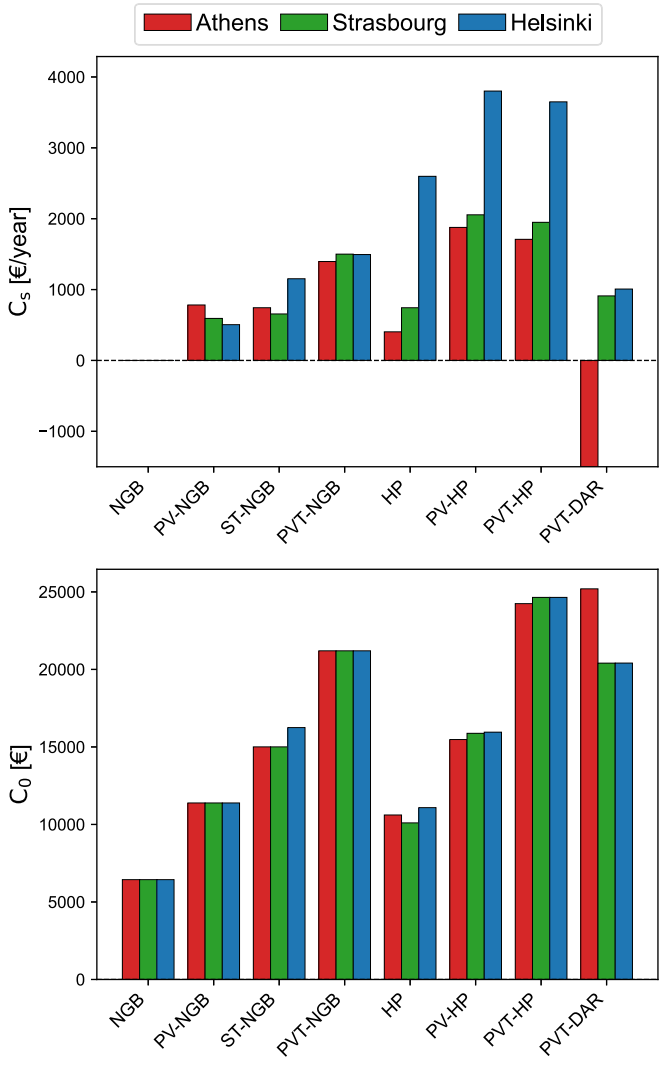

Fig. 15. Initial investment costs and C_s for various system combinations in selected cities. C_s values for H. Boiler (−3480, −4470, − 2785 €/year for Athens, Strasbourg, Helsinki, respectively) and PVT-DAR (−5940 €/year for Athens). These values are not fully displayed to show other values clearly.

operational costs (0.078–0.135 €/kWh) due to solar electricity generation offsetting heat pump consumption.The PVT-HP system, while offering dual thermal and electrical output capabilities, demonstrate a higher $LCOE_{eq,el}$ compared to their PV-HP counterparts, approximately 26 % higher in Athens and 39 % higher in Strasbourg compared to the PV-HP system. This is primarily driven by higher capital costs (0.110–0.116 €/kWh) rather than operational inefficiencies, as operational costs remain competitive (0.089–0.146 €/kWh). This is primarily due to the higher capital costs associated with PVT collectors. Thus, PVT system's higher upfront investment partially offsets some of the benefits of integrated thermal energy production, resulting in a slightly less competitive cost structure.

The hydrogen boiler system has the same cost as the natural gas boiler system but exhibits significantly higher $LCOE_{eq,el}$, 44 % in Helsinki and 100 % in Athens compared to the stand-alone natural gas system. This is because of the current high production and distribution costs of hydrogen relative to natural gas which increases the operational

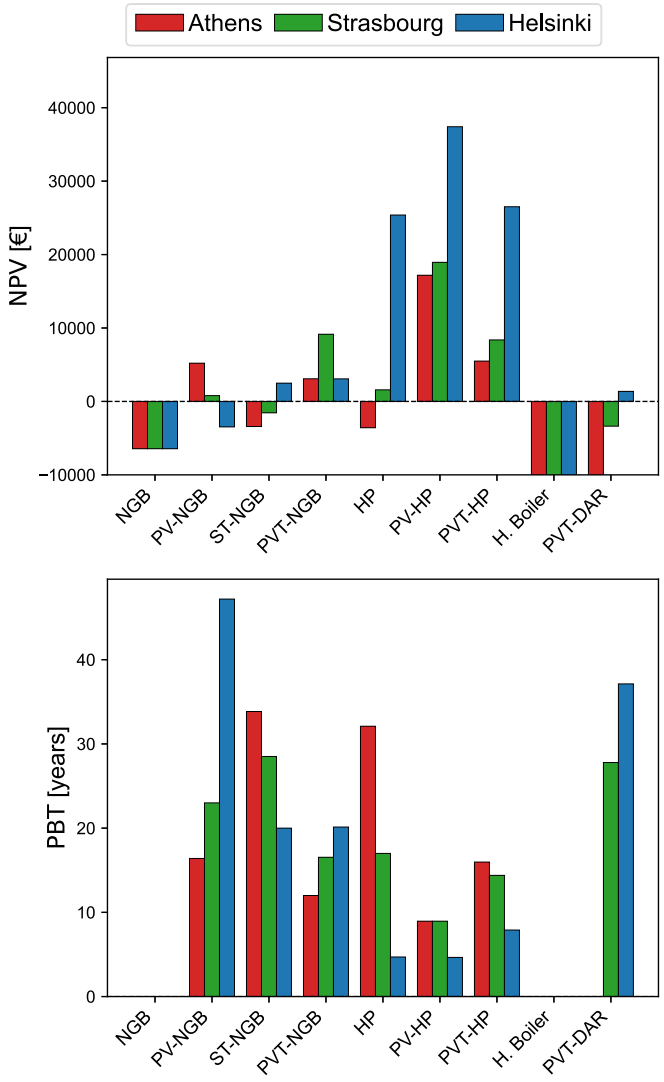

Fig. 16. NPV and PBT for various system combinations in selected cities. NPV values for H. Boiler (−49,865, − 61,615, −36,535 €/year for Athens, Strasbourg, Helsinki, respectively) and PVT-DAR (−151,110 €/year for Athens) are not fully displayed to show other values clearly.

expenses of the hydrogen boiler system. While these elevated costs highlight the economic challenges facing hydrogen boilers, future advancements in green hydrogen technology could reduce these costs, enhancing the competitiveness of hydrogen boilers.

When it comes to PVT-DAR systems, the primary challenge in Athens was the high cooling demand, which directly increased the number of DAR units required and, consequently, the number of generators needed, resulting in both high capital costs (0.160 €/kWh) and operational costs (0.950 €/kWh). In contrast, for Strasbourg and Helsinki, the results were not as pessimistic as those observed for Athens, with capital costs of 0.147 and 0.195 €/kWh respectively, and significantly lower operational costs (0.145 and 0.106 €/kWh).

Cost savings (C_S) do not consider the initial investment costs (C_0) and focus exclusively on operational savings. As a result, the differences between PVT-based systems and their corresponding PV systems are minimized, or in some cases, PVT-based systems appear more favorable since they cover both electrical and heat demand. However, while PV prices have decreased significantly over the past decade, PVT prices have remained relatively stable, making PVT systems less competitive from a capital cost perspective. To enhance the competitiveness of PVT systems, further research and development efforts are crucial to reduce manufacturing costs.

The cost savings of HPs exhibit significant regional variations, ranging from 403 €/year in Athens to 2598 €/year in Helsinki. This can be explained by the electricity-to-gas price ratio, which is highest in Greece (2.48) and lowest in Finland (1.19), reflecting the relative affordability of electricity compared to natural gas in these regions. A higher electricity-to-gas price ratio makes heat pumps less economically attractive, as they rely on electricity for operation. Conversely, lower ratios, as seen in Finland, enhance the cost-effectiveness of heat pumps. Furthermore, there is a strong correlation between heat pump sales per 1000 households and the electricity-to-gas price ratio [100]. While it is not the sole factor influencing heat pump adoption, this price ratio offers a compelling explanation for the regional variations in cost savings.

Figure 16 shows the NPV results for the evaluated systems. The boiler system showing a negative NPV because it does not generate cost saving. Similarly, systems such as PV-NGB, ST-NGB, and PVT-NGB exhibit low or negative NPV values, as the calculations account for all system components, including the boiler and AC.

When looking at the HP system, the NPV varies significantly depending on regional energy price structures. In Athens, the HP system demonstrates a negative NPV (−3580 €), primarily attributed to the region's low natural gas prices, which diminish the economic advantage of adopting this technology. Conversely, in Helsinki, where natural gas prices are 2.37 times higher than Athens, the HP system achieves a more favorable NPV (25,380 €). The results for the hydrogen boiler and PVT-DAR systems align with the previously explained trends. Notably, the PV-HP system emerges as the most economically viable option across all analyzed cities, achieving the highest NPV.

When it comes to PBT, it is important to note that negative values indicate an inability to recover initial investment costs within the analyzed timeframe. The boiler system serves as a benchmark and does not have a PBT, as it does not generate cost savings to offset the initial investment. Furthermore, PBT varies across regions due to differences in cost savings. The PV-HP system is the most favorable for all analyzed cities. In Finland, where PV-HP system cost savings are highest, it achieves a shorter PBT of 4.65 years, while in Greece, where cost savings are lower, the PBT extends to 8.95 years.

The Internal Rate of Return (IRR) analysis was also calculated and results are shown in Fig. 17. IRR is the discount rate at which the NPV of the investment equals zero, with results aligning with NPV trends previously discussed. NGB based systems exhibit lower returns, with PVT-NGB showing a moderate IRR (5–6 %), due to complete system costs including boiler and AC components, reduce overall system profitability. In Athens, the standalone HP system achieves only 0.2 % IRR due to low natural gas prices, consistent with its negative NPV performance. However, PV-HP systems show strong viability at 13.3 % IRR in the same location. In Strasbourg, the PV-HP system leads with 14.1 % IRR, followed closely by the PV-HP system at 7.3 %. Helsinki presents the most favorable economic environment for heat pump technologies due to high natural gas prices, with the HP system achieving 23.6 % IRR and the PV-HP system reaching the highest IRR of 24.0 % across all configurations and locations."

3.4. Comparative analysis under variable energy source prices

Analyzing the system profitability sensitivity to variations in natural gas (or hydrogen) and electricity prices is particularly important.

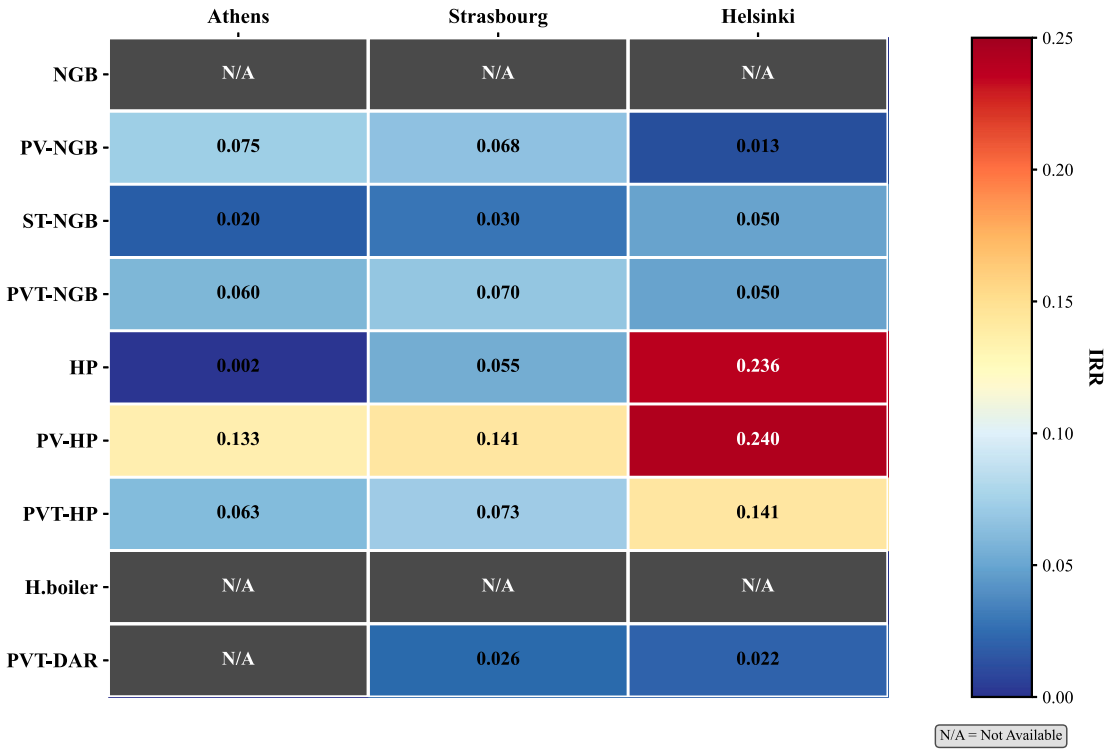

Fig. 17. IRR for evaluated system configurations in Athens, Strasbourg, and Helsinki.

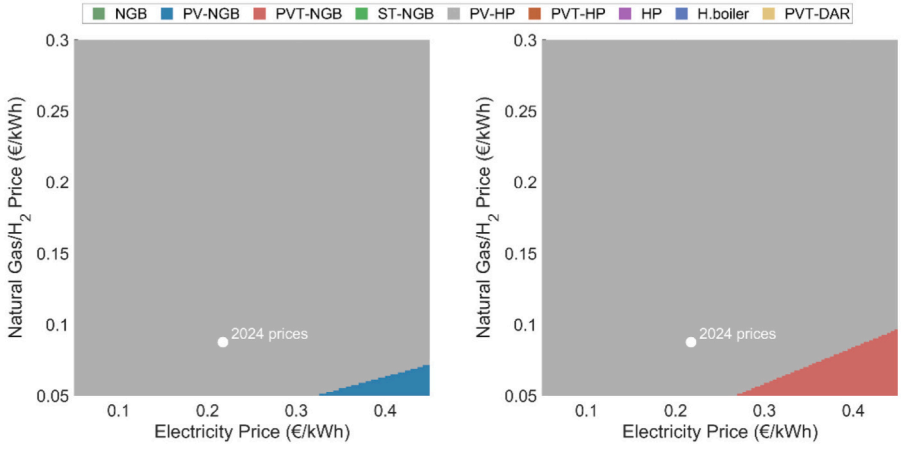

Fig. 18. Comparison of technologies based on: (a) lowest $LCOE_{eq,el}$ and (b) highest C_s across varying electricity and gas prices (natural gas or hydrogen) for Athens. Different colors indicate which combination is the most favorable for a given combination of prices.

Figs. 18 – 20 show which technology achieves the lowest $LCOE_{eq,el}$ (Figs. 18(a), 19(a) and 20(a)) for each price combination for the analyzed cities. The overall trends remain consistent, but slight variations arise due to differences such as in local climate and energy price structures. The PV-HP system is the most economically advantageous option across a wide range of price combinations. This is due to the system leveraging both solar electricity generation and its efficient use via heat production through the heat pump, making it highly competitive. In contrast, the PV-NGB system (PV + natural gas boiler + AC) demonstrates competitiveness only under very low natural gas prices and high electricity prices, where the boiler remains cost-effective for heating, and the PV system reduces electricity-related costs.

Figs. 18(b), 19(b) and 20(b) show which technology achieves the highest cost saving for each price combination for analyzed cities. Unlike the $LCOE_{eq,el}$ analysis, this metric does not account for the initial capital cost (C_0) and focuses solely on operational savings. Thus, it provides additional insights into system performance. The results largely align with $LCOE_{eq,el}$with one key difference: the PVT-NGB system (PVT

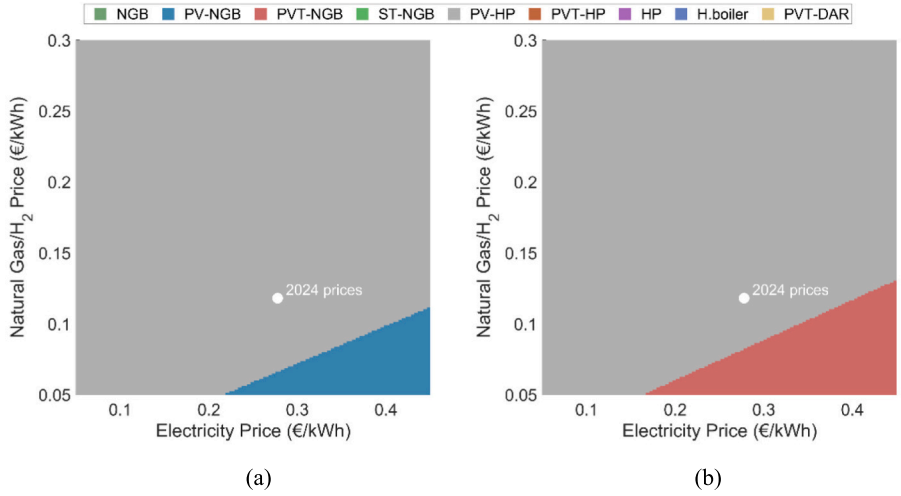

Fig. 19. Comparison of technologies based on: (a) lowest $LCOE_{eq,el}$ and (b) highest C_s across varying electricity and gas prices (natural gas or hydrogen) for Strasbourg. Different colors indicate which combination has the most favorable for a given combination of prices.

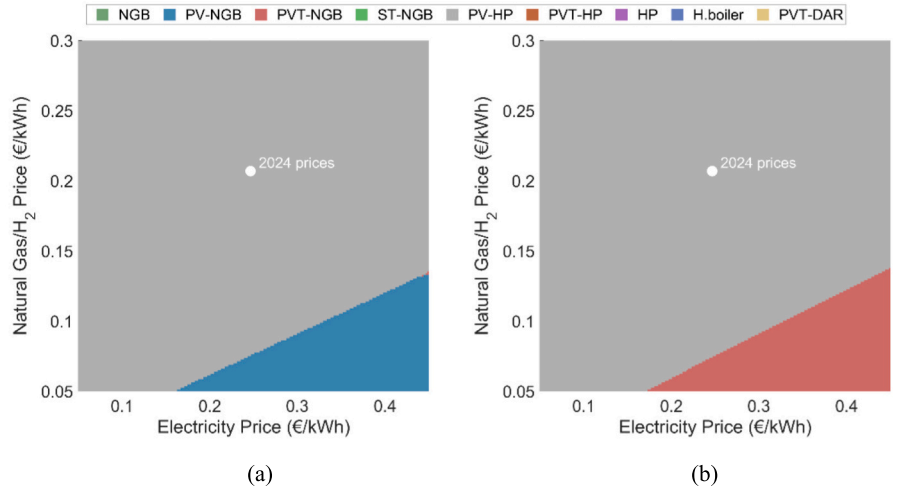

Fig. 20. Comparison of technologies based on: (a) lowest $LCOE_{eq,el}$ and (b) highest C_s across varying electricity and gas prices (natural gas or hydrogen) for Helsinki. Different colors indicate which combination has the most favorable for a given combination of prices.

+ natural gas boiler + AC) achieves the highest cost savings within a narrow band of very low gas prices and high electricity prices. Despite its high initial capital cost, the PVT system's combined production of electricity and heat leads to greater operational savings.

Systems heavily reliant on a single energy resource (e.g., natural gas or electricity) perform poorly when that resource becomes expensive. In contrast, systems with solar energy (e.g., PVT-NGB or PV-HP) remain competitive even when main heating systems (such as boilers or heat pump) become less economical due to rising prices. Similarly, technologies like hydrogen-based systems are not viable due to expensive hydrogen supplies, limiting their applicability. Emerging technologies, such as DAR, face higher costs due to lack of economies of scale compared to established options like conventional AC. These factors explain why certain technologies do not appear as optimal or cost-saving across broader scenarios.

For demonstration purposes, we also present a separate figure, Fig. 21, for the same results excluding the PV-HP system for the selected cities. This allows a more detailed examination of performance characteristics of the remaining systems and offering a more nuanced understanding of their potential viability under different energy market conditions. The figure indicates that the optimal system selection is highly sensitive to both electricity and gas prices. Understanding the interplay between these prices is important for long-term energy planning. Under 2024 prices, in Helsinki, the PVT-HP system has the lowest $LCOE_{eq,el}$. In Athens, it remains the dominant choice across a broad range of price scenarios benefiting from its warmer climate and the contribution of PVT systems for both electricity and heat generation. The HP-only option is competitive at lower electricity prices, where in Helsinki it extends over a wider range. This highlights the importance of efficient heat pumps in cold climates.

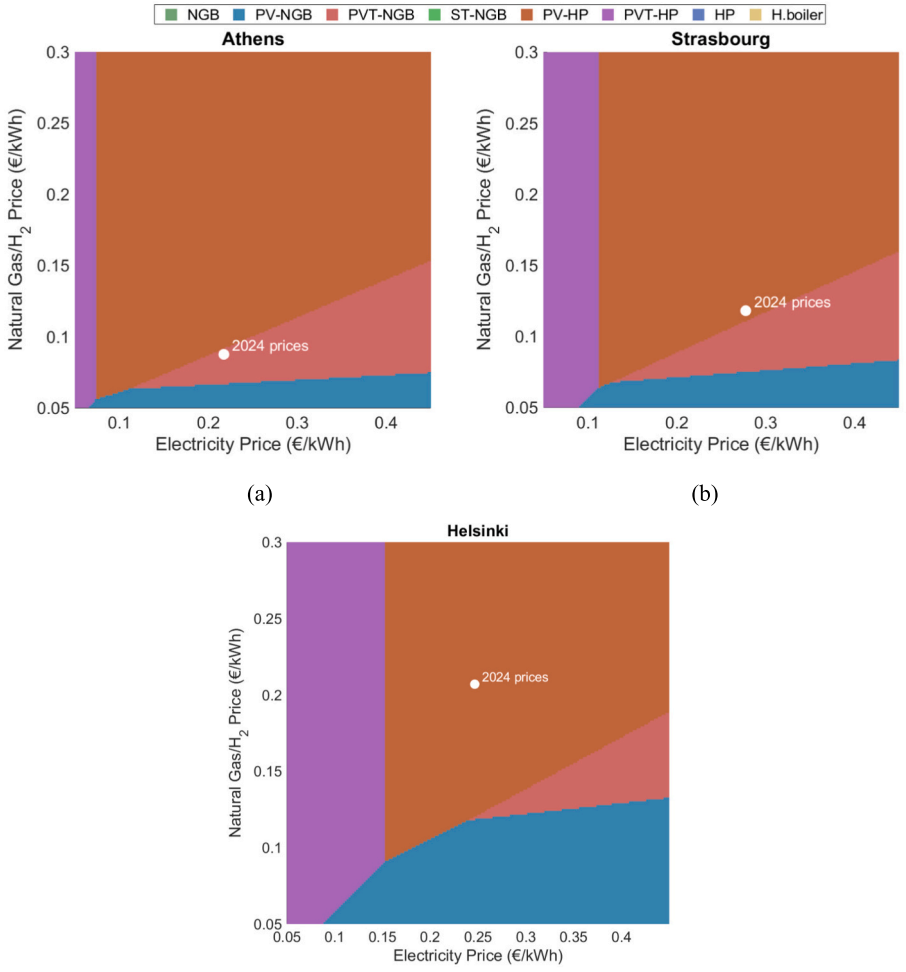

Fig. 21. Comparison of technologies based on lowest $LCOE_{eq,el}$, excluding the PV-HP system, across varying electricity and gas prices (natural gas or hydrogen depend on system) for: (a) Athens; (b) Strasbourg; and (c) Helsinki. Different colors indicate which combination has the most favorable for a given combination of prices.

4. Conclusions

In this study, the techno-economic potential of various heating, cooling, and power generation systems for residential buildings was investigated across different climates in Europe, focusing on Athens, Strasbourg, and Helsinki. The systems included combinations of the following technologies: PV, ST, PVT, HP, natural gas boiler, hydrogen boiler, AC, and DAR. Nine different combinations were proposed to meet residential energy demands: (1) PVT + HP + AC; (2) PV + HP + AC; (3) HP + AC; (4) Natural gas boiler + AC; (5) PV + natural gas boiler + AC; (6) ST + natural gas boiler + AC; (7) PVT + natural gas boiler + AC; (8) Hydrogen boiler + AC; and (9) PVT + DAR system, with natural gas boiler as a backup. Transient MATLAB models were developed for each system configuration, solved using hourly electricity, heating, and cooling demand profiles for three locations with distinct weather and resource price characteristics. These models enabled economic, environmental, and energetic analysis, facilitating a comparative assessment of the different systems' performance. The study aimed to determine the optimal system configurations for single-family homes in varying climatic conditions.

The key results of this analysis are presented below:

- The performance of solar technologies varied considerably depending on the local climate and the specific technology used. For example, the PVT-NGB system's electricity coverage was 53.0 % in Athens and 39.5 % in Helsinki.
- PV technologies effectively resulted in lower CO_2 emissions in Athens, where grid electricity emissions were consistently 2 to 5 times higher than in Strasbourg or Helsinki. Consequently, the environmental benefits of PV technologies in Athens were more pronounced compared to Strasbourg and Helsinki.
- The PV-HP system combination demonstrated the highest emission reduction in Athens, achieving 4700 kg $CO_{2,eq}$/year, followed closely by the PVT-HP system with a difference of approximately 300 kg $CO_{2,eq}$/year. In Strasbourg and Helsinki, both PV-HP and PVT-HP systems exhibited similar emission reductions of 4200 and 3900 kg $CO_{2,eq}$/year, respectively, albeit lower than those observed in Greece due to regional differences in the carbon intensity of grid electricity. Notably, the hydrogen boiler achieved the highest emission reduction in Strasbourg and Helsinki (4270 kg $CO_{2,eq}$/year), driven by the use of green hydrogen in this analysis, which entails no direct emission and higher heating demands in both cities.
- Integrating heat pumps with solar technologies (e.g., PVT-HP and PV-HP systems) showed significant potential to enhance energy efficiency and dependence on grid electricity. These systems were able

to meet a significant portion of heating demand while minimizing operating costs. In terms of $LCOE_{eq,el}$, the PV-HP system consistently achieved the lowest $LCOE_{eq,el}$ across all cities, ranging from 0.1446 €/kWh in Athens to 0.2028 €/kWh in Strasbourg, followed by PVT-HP (approximately 26 % percent higher in Athens and 39 % higher in Strasbourg compared to PV-HP). The higher initial cost of PVT systems compared to PV systems contributed to the slightly higher $LCOE_{eq,el}$ values despite their dual thermal and electrical output capabilities.

- Hydrogen boilers fueled by green hydrogen exhibited higher $LCOE_{eq,el}$ values, reaching twice in Athens and Strasbourg and approximately 40 % higher in Helsinki, despite high natural gas prices in Finland. The economic viability of hydrogen boilers in the future will largely depend on advancements in green hydrogen production and distribution, which could reduce costs and improve their competitiveness as a sustainable heating solution.
- The cost savings associated with heat pumps varied significantly across regions, ranging from 403 €/year in Athens to 2598 €/year in Helsinki. This variation can be attributed to the electricity-to-gas price ratio, which is highest in Greece (2.48) and lowest in Finland (1.19). This price ratio provides a compelling explanation for the regional variations in cost savings and, consequently, technology adoption. Furthermore, the PV-HP system achieved a lower PBT of 4.65 years in Finland and 8.95 years in Greece.

Several directions for future research emerge from this study's findings and limitations. This study focused on grid-connected configurations without battery energy storage systems (BESS) to maintain a manageable framework for comparing heating and cooling technologies across diverse climates. Future research should integrate BESS to enhance solar energy utilization, self-consumption, and grid flexibility.

The techno-economic feasibility of hydrogen-based heating solutions requires deeper investigation in future work. This analysis should consider various hydrogen production methods (e.g., blue hydrogen with carbon capture and storage) and their associated infrastructure costs. A comprehensive analysis of transition pathways (e.g., blending scenarios with natural gas, regional infrastructure challenges) is essential.

While this study focused on the like-to-like comparisons, integrating demand-side management (DSM) strategies is a key area for further research to optimize residential energy systems. For PV systems, DSM can include load shifting to better align electricity consumption with periods of solar generation, thereby increasing self-consumption and reducing grid reliance. For PVT and ST systems, coordinated control of thermal storage (e.g., hot water tanks) can store excess solar energy during the day and offset auxiliary heating needs during non-solar hours, improving solar utilization. For HP systems, load shifting based on dynamic electricity tariffs or renewable energy forecasts can lower operational costs and improve overall system efficiency. Hybrid HP–boiler systems can operate flexibly by prioritizing heat pump use during low-tariff or renewable-rich periods, with boilers providing backup during high-demand or low-renewable conditions. For AC systems, the building thermal mass can be exploited to pre-cool indoor spaces during off-peak hours, further supporting DSM goals.

Future research should extend the current comparative analysis by incorporating multi-objective optimization techniques that offer tailored solutions to identify optimal system configurations under different priorities such as minimizing cost, reducing emissions, or maximizing energy efficiency. This approach would enhance decision-making support for both policymakers and system designers in diverse climatic and regulatory contexts. Additionally, future research should build upon the current analysis by incorporating scenarios that reflect projected trends in climatic conditions and grid decarbonization, as well as risk-based analyses to capture uncertainties in key parameters. Also, national or region-specific support schemes should be integrated to provide a more comprehensive picture of deployment feasibility and to better inform policy-relevant techno-economic comparisons under different regulatory frameworks.

The environmental assessment in this study focused on operational CO_2 emissions, but a comprehensive environmental evaluation should encompass broader considerations. Future research should incorporate full Life Cycle Assessment methodologies to quantify embodied energy from manufacturing, transportation impacts, and end-of-life considerations such as refrigerant management and material recovery. Such comprehensive analysis would provide stakeholders with more complete environmental decision-making tools while supporting policy development for sustainable energy system deployment.

It is important to note that the identified economic optimal configurations represent the best among the nine specific system combinations studied under the stated conditions. Further research exploring alternative configurations outside the scope of this study may show addtional interesting insights. For the integrated PVT - heat pump system, different configurations can be studied to increase energetic performance. When it comes to the DAR system, different refrigerant fluid pairs and backup systems can be investigated to improve their efficiency and environmental compatibility. Furthermore, future research could examine the influence of variations in solar availability and heating/cooling loads to broaden the scope of our findings.

CRediT authorship contribution statement

Mustafa Kurses: Software, Validation, Investigation, Writing – original draft, Methodology. **Andreas V. Olympios:** Validation, Data curation, Writing – review & editing, Formal analysis, Investigation. **Asmaa A. Harraz:** Methodology, Resources, Writing – review & editing, Investigation. **Jingyuan Xu:** Project administration, Conceptualization, Supervision, Funding acquisition, Writing – review & editing, Methodology.

Declaration of competing interest

The authors declare that they have no known competing financial interests or personal relationships that could have appeared to influence the work reported in this paper.

Acknowledgments

The authors gratefully acknowledge the support provided by the Carl-Zeiss-Stiftung, the Baden-Wurttemberg Stiftung, and the Hector Fellow Academy.

Appendix A

A.1. Coil type heat exchanger

All the symbols defined in the main body of this paper are not redefined here. The reader is directed to the nomenclature for symbol definitions.

The thermal resistance term, needed for the NTU method, is calculated using Eq. A.1:

$$R_{\text{coil}} = \frac{d_o}{d_i h_{\text{coil}}} + \frac{ln\left(\frac{d_o}{d_i}\right)}{2\pi L_{\text{coil}} k_p} + \frac{1}{h_t} \tag{A.1}$$

where h_{coil}, h_t are heat transfer coefficients in the coil for forced convection and the coefficient in the tank for natural convection, respectively. L_{coil} is the length of the coil. k_p is thermal conductivity of the copper pipe of the coil (set to 385 W m^{-1} K^{-1}).

Correlations for the forced convection in the coil-type heat exchanger [101], and in the tank [102] obtained from Eq. A.2 and A.3 respectively:

$$h_{\text{tank}} = \frac{Nu_{\text{tank}} k_{\text{water}}}{d_o} \tag{A.2}$$

$$h_{\text{coil}} = \frac{Nu_{\text{coil}} k_{\text{water}}}{d_i} \tag{A.3}$$

where d_i and d_o are the internal and external diameters of the coil, respectively.

The Nusselt number for forced convection in the coil-type heat exchanger and the Nusselt number for natural convection heat transfer coefficient inside the water tank [102] are calculated using Eq. A.4 and A.5, respectively:

$$Nu_{\text{coil}} = \begin{cases} 3.66 + 0.08\left(1 + 0.8\left(\frac{d_i}{d_o}\right)^{0.9}\right)(Re_{coil})^m (Pr)^{0.3}, if Re_{\text{coil}} < Re_{\text{critic}} \\ 0.023(Re_{\text{coil}})^{0.85}(Pr)^{0.4}, if\ Re_{\text{coil}} \geq Re_{\text{critic}} \end{cases} \tag{A.4}$$

$$Nu_{\text{tank}} = 0.52(Ra_{\text{tank}})^{0.25} \tag{A.5}$$

The Prandtl number corresponds to the water circulating through the coil, while m is a coefficient related to the coil diameters.

The Reynolds number for the flow in the coil and correlation for estimation of the critical Reynolds number are obtained with Eq. A.6 and A.7 respectively:

$$Re_{\text{coil}} = \frac{\dot{m}_{\text{fa}}}{\frac{\pi}{4} d_i \mu} \tag{A.6}$$

$$Re_{\text{critic}} = 2300\left[1 + 8.6\left(\frac{d_i}{d_o}\right)^{0.45}\right] \tag{A.7}$$

where μ the dynamic viscosity of water, in Pa•s.

Prandtl number is determined by:

$$Pr = \frac{c_p \mu}{k_{\text{water}}} \tag{A.8}$$

The coefficient, m, for the coil diameters is calculated by:

$$m = 0.5 + 0.29\left(\frac{d_i}{d_o}\right)^{0.19} \tag{A.9}$$

The Rayleigh number for the water in the tank is calculated by:

$$Ra_{\text{tank}} = \frac{g\beta|T_{\text{mf}} - T_{\text{wt}}|(d_o)^3}{\nu\alpha} \tag{A.10}$$

β is the thermal volume expansion in $^\circ C^{-1}$, ν is the kinematic viscosity, α is the thermal diffusivity of the water inside the tank, and g is the acceleration due to gravity.

A.2. Circulation pump power

The power consumption of the PVT circulation pump is given by eq. A.11 [101,103].

$$P_{\text{pump}} = \frac{\dot{m}_{\text{fa}}(\Delta P_{\text{collector}} + \Delta P_{\text{PVT}})}{\eta_{\text{pump}}\rho_{\text{water}}} \tag{A.11}$$

where $\Delta P_{\text{collector}}$, ΔP_{PVT} Pressure drops in PVT collectors and circulation loop, respectively, in Pa. η_{pump} is pump efficiency (set to 85 %) and ρ_{water} is the density of water.

The pressure drops in the PVT circulation loop are calculated using eq. A.12:

$$\Delta P_{\text{PVT}} = \frac{fL_{\text{pipe}}}{D_{\text{h}}} 0.5\rho \left(\frac{\dot{m}_{\text{fa}}}{\rho A_{\text{pipe}}} \right)^2 \tag{A.12}$$

where f is the friction factor, determined as indicated in [104]. L_{pipe}, D_h, A_{pipe} are length, hydraulic diameter, and internal area of the pipes in the loop system, respectively.

The pressure drop in each collector is assumed to be constant at 180 mbar, which is the average of values reported in previous studies [105,106].

$$\Delta P_{\text{collector}} = 0.18 \bullet 10^5 Pa \tag{A.13}$$

A.3. Cost saving equations for each system

The calculation of C_s depends on the system considered. For PVT-HP, PV-HP, and HP systems, it is calculated using:

$$C_{\text{s}} = C_{\text{O\&M,boiler}} - C_{\text{O\&M}} + (E_{\text{cov}} - E_{\text{HP,uncov}})c_{\text{e}} + E_{\text{exc}}s_{\text{e}} + \frac{(Q_{\text{DHW,cov}} + Q_{\text{SH,cov}})c_{\text{ng}}}{\eta_{\text{boiler}}} \tag{A.14}$$

For PVT-NGB, PV-NGB, and ST-NGB systems, it is calculated using:

$$C_{\text{s}} = -C_{\text{O\&M}} + (E_{\text{app,cov}})c_{\text{e}} + E_{\text{exc}}s_{\text{e}} + \frac{(Q_{\text{HW,cov}} + Q_{\text{SH,cov}})c_{\text{ng}}}{\eta_{\text{boiler}}} \tag{A.15}$$

For PVT-DAR system's C_s is calculated uinsg:

$$C_{\text{s}} = C_{\text{O\&M,boiler}} - C_{\text{O\&M}} + (E_{\text{app,cov}} + E_{\text{sc,cov,eqel}})c_{\text{e}} + E_{\text{exc}}s_{\text{e}} + \frac{(Q_{\text{HW,cov}} + Q_{\text{SH,cov}} - Q_{\text{heater}})c_{\text{ng}}}{\eta_{\text{boiler}}} \tag{A.16}$$

where, $E_{\text{sc,cov,eqel}}$ is the covered SC demand with DAR system, and Q_{heater} is an additional heat from the water heater required to provide the energy needed for the operation of the DAR system.

C_s for hydrogen boiler is equal to:

$$C_{\text{s}} = \frac{(Q_{\text{HW}} + Q_{\text{SH}})c_{\text{ng}}}{\eta_{\text{boiler}}} - \frac{(Q_{\text{HW}} + Q_{\text{SH}})c_{\text{H}}}{\eta_{\text{H.boiler}}} \tag{A.17}$$

Here, c_{H} is the cost of hydrogen price.

A.4. Cost estimation equations

For systems that use PVT, piping costs for pipes needed for PVT system are estimated as a function of the total area occupied, and the pipe diameter used for heat transfer fluid circulation:

$$I_{\text{pipe}} = 4\sqrt{A_{\text{c,total}} + 40} \bullet (0.897 + 0.21D_{\text{pipe}}) \tag{A.18}$$

Also, heat transfer fluid costs, circulating in PVT, are determined by the total volume required:

$$I_{\text{htf}} = 3.3V_{\text{htf}} \tag{A.19}$$

where V_{htf} is the volume of heat transfer fluid to be used.

The HTF pump cost is estimated by [107]:

$$I_{\text{pump}} = 500\left(\dot{W}_{\text{pp}} \Big/ 300 \right)^{0.25} \tag{A.20}$$

where $\dot{W}_{\text{pp}}$ is the peak electrical power of the pump, in W.

Also, as an auxiliary equipment cost, the controller and expansion vessel are assumed 110 and 140 euros, respectively [45].

A.5. Model validation of PVT system

The next figure represents the validation of the PVT panel model, showing the comparison between simulated and experimental thermal efficiency.

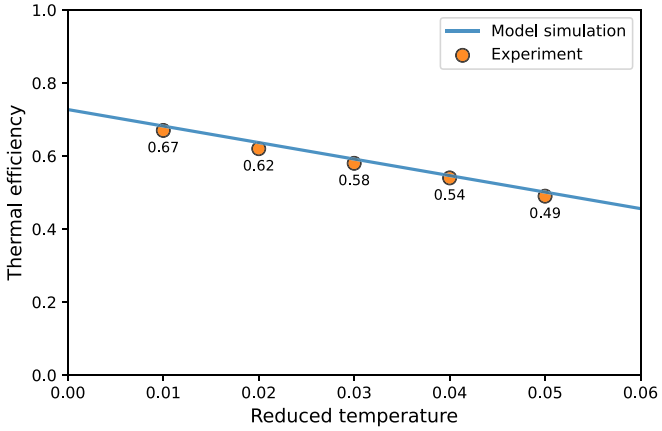

Fig. A1. Validation of the photovoltaic-thermal (PVT) panel model against experimental data. The blue line represents the simulated thermal efficiency of the PVT panel according to Eq. (1), plotted as a function of reduced temperature. The red squares indicate actual experimental measurements. The close agreement between the two confirms the accuracy of the PVT model. The experimental data were obtained from Ref. [108]

A.6. DAR model description

A description of this process can be summarized:

- The PVT system produces residual heat, which is transferred to the refrigerant-rich solution (1) in the generator. This heat $(\dot{Q}_{\text{gen}})$ causes the solution to boil (2).
- The rising bubbles lift the solution through the inner tube of the bubble pump. At the top of the tube, the refrigerant vapor (4) is separated from the weak refrigerant solution (3), which returns downwards.
- The refrigerant vapor that rises from the bubble pump may not be pure enough to go directly to the condenser (When using water or a similar relatively volatile absorbent), and should pass through a rectifier. In the rectifier, more refrigerant is purified by releasing heat $\left(\dot{Q}_{rec}\right)$ to the environment.
- The purified refrigerant vapor (6) enters the condenser, where it loses heat $\left(\dot{Q}_{cond}\right)$ to the ambient and changes into a liquid state.
- After being subcooled through a gas heat exchanger, the nearly pure refrigerant enters the evaporator (7). In the evaporator, the liquid refrigerant encounters the auxiliary gas (8,g) (hydrogen), leading to evaporation due to the lower partial pressure. This evaporation absorbs heat $(\dot{Q}_{\text{evap}})$ from the space being cooled, which defines the cooling capacity of the system. After leaving the evaporator (10), the refrigerant-auxiliary gas mixture is directed to the reservoir.
- The refrigerant-auxiliary gas mixture enters the absorber, where it contacts the weak refrigerant solution. The refrigerant is absorbed into the solution, releasing heat $\left(\dot{Q}_{abs}\right)$, while the incondensable auxiliary gas moves up the absorber and returns to the evaporator through the gas heat exchanger.
- The refrigerant-strong solution returns to the generator (11), preheated in a solution heat exchanger by the weak solution returning from the absorber (1), thus closing the cycle.

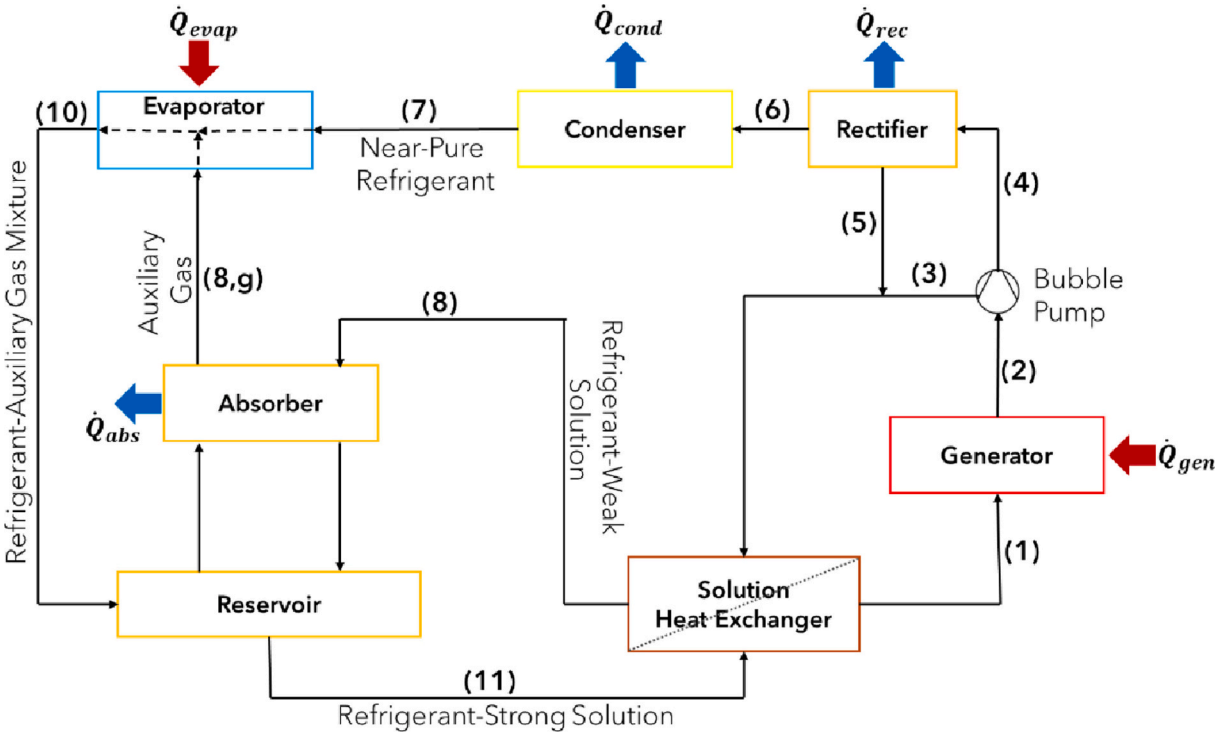

Fig. A3. A simple block diagram of a DAR system. This figure was adapted with permission from Ref. [30]

A.7. Additional tables and figures.

Table A1
Overview of annual electricity and heat performance of different system combinations across three countries. Table presents yearly heat demand (Q_{dem}), heat input to the tank via direct solar thermal energy ($E_{cov,\ app}$), and solar-sourced electricity used by the heat pump ($Q_{cov,HP}$), yearly electricity demand (E_{dem}), solar-sourced electricity contributions for the heat pump ($E_{cov,HP}$) and household appliance electricity demand ($E_{cov,\ app}$). All values are in kWh.

Country	System	Electricity			Heat		
		$E_{cov,app}$	$E_{cov,HP}$	E_{DEM}	Q_{DEM}	$Q_{th,solar}$	$Q_{COV,HP}$
	PV-NGB	1662	–	3000	12,719	0	–
	PVT-NGB	1589	–	3000	12,719	4872.7	–
Athens	ST-NGB	0	–	3000	12,719	6527.5	–
	PV-HP	1563	1879	7236	12,719	–	6750
	PVT-HP	1681	1195	6633	12,719	2772	4070
	PV-NGB	1412	–	2872	17,391	0	–
	PVT-NGB	1346	–	2872	17,391	4519.7	–
Strasbourg	ST-NGB	0	–	2872	17,391	5733	–
	PV-HP	1333	1858	9061	17,391	–	6357
	PVT-HP	1412	1321	8618	17,391	1934	4308
	PV-NGB	1092	–	2659	17,393	0	–
	PVT-NGB	1030	–	2659	17,393	3225.2	–
Helsinki	ST-NGB	0	–	2659	17,393	5337.6	–
	PV-HP	1023	1742	9779	17,393	–	5398
	PVT-HP	1070	1366	9491	17,393	1193	4064

The COP of a HP increases as the temperature difference between the hot sink and the cold source decreases. Since the temperature difference at the water tank (T_{WT}) varies by no more than 10 °C when the heat pump is activated, the COP is mainly influenced by the ambient temperature. The peak COP typically occurs at the warmest point of the year, depending on the location.

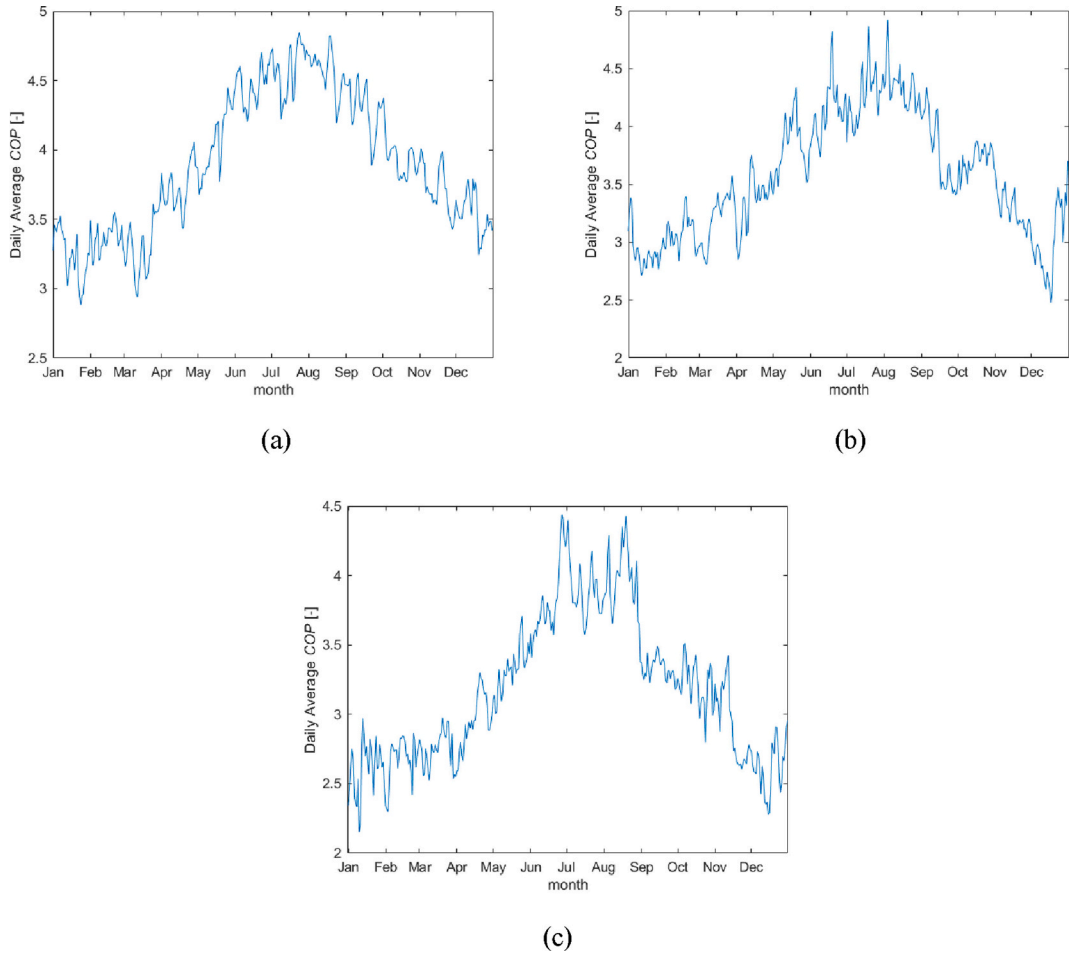

Fig. A4. Daily average COP of HPs throughout the year for: (a) Athens; (b) Strasbourg; and (c) Helsinki.

A.8. Additional system specifications of simulated systems

HP system: The capacity of HP is set to 5.5 kW, with design temperatures of 2 °C for Athens, −3.2 °C for Strasbourg, and − 10.3 °C for Helsinki. These temperatures represent the 99th percentile values, meaning they were exceeded only 1% of the time in 2023 as recorded by meteorological stations in the three studied cities.

Water storage tank: A nominal volume of 744 L was used consistently across all simulations.

AC System: The AC units were sized to meet the peak cooling demand for each climate zone, with capacities of 4 kW, 3 kW, and 2.5 kW for Athens, Strasbourg, and Helsinki, respectively.

DAR System: The DAR system's cooling capacity was selected to match the peak cooling requirements of each location. This resulted in cooling capacities 4 kW, 3 kW, and 2.5 kW for Athens, Strasbourg, and Helsinki, respectively.

Data availability

The data supporting the findings of this study are available from the corresponding author upon reasonable request. Additionally, numerical model details used in this study can be accessed upon request, provided they comply with institutional and funding body requirements.

References

[1] CO2 Emissions in 2022 – Analysis. International Energy Agency (IEA). https://www.iea.org/reports/co2-emissions-in-2022. [Accessed 15 October 2024].
[2] Directive (EU) 2024/1275 of the European Parliament and of the Council of 24 April 2024 on the energy performance of buildings (recast) (Text with EEA relevance). http://data.europa.eu/eli/dir/2024/1275/oj/eng. [Accessed 15 October 2024].
[3] Maduta C, Melica G, D'Agostino D, Bertoldi P. Towards a decarbonised building stock by 2050: the meaning and the role of zero emission buildings (ZEBs) in Europe. Energ Strat Rev 2022;44:101009. https://doi.org/10.1016/j.esr.2022.101009.
[4] Energy use in EU households in 2022 lowest since 2016. Eurostat; 2024. https://ec.europa.eu/eurostat/web/products-eurostat-news/w/ddn-20240605-2. [Accessed 15 October 2024].
[5] World Energy Outlook 2022 – Analysis. IEA. https://www.iea.org/reports/world-energy-outlook-2022. [Accessed 15 October 2024].
[6] Granryd E. Refrigerating engineering. Stockholm, Sweden: Royal Institute of Technology, KTH, Department of Energy Technology, Division of Applied Thermodynamics and Refrigeration; 2009.
[7] Heat supply, Nor. Energy (n.d.), https://energifaktanorge.no/en/norsk-energiforsyning/varmeforsyning/. [Accessed 22 October 2024].
[8] Hirvonen Jussi. Finland: Heat pump market outlook. Finnish Heat Pump Association; 2021. https://heatpumpingtechnologies.org/publications/finland-heat-pump-market-outlook/. [Accessed 22 October 2024].
[9] European Hydrogen Backbone. How a dedicated Hydrogen infrastructure can be created. Utrecht: The Netherlands; 2020. https://www.newenergycoalition.org/custom/uploads/2020/10/European-Hydrogen-Backbone-Report.pdf.

[10] Quintino FM, Nascimento N, Fernandes EC. Aspects of Hydrogen and biomethane introduction in natural gas infrastructure and equipment. Hydrogen 2021;2:301–18. https://doi.org/10.3390/hydrogen2030016.

[11] UNECE. Technology Brief Hydrogen. United Nations economic Commission for Europe Task Force on Hydrogen, Geneva. https://unece.org/sites/default/files/2022-02/Hydrogen%20brief_EN_final.pdf; 2021.

[12] Klopčič N, Stöhr T, Grimmer I, Sartory M, Trattner A. Refurbishment of natural gas pipelines towards 100% Hydrogen—a thermodynamic-based analysis. Energies 2022;15:9370. https://doi.org/10.3390/en15249370.

[13] Trinomics, Opportunities for Hydrogen energy technologies considering the National Energy & Climate Plans. Fuel Cells and Hydrogen Joint Undertaking; 2020. https://www.lei.lt/wp-content/uploads/2020/09/Final-Report-Hydrogen-in-NECPs-28-8-2020-ID-9474232.pdf.

[14] Incer-Valverde J, Korayem A, Tsatsaronis G, Morosuk T. "Colors" of hydrogen: definitions and carbon intensity. Energy Convers Manag 2023;291:117294. https://doi.org/10.1016/j.enconman.2023.117294.

[15] Geopolitics of the energy transformation: The hydrogen factor. Abu Dhabi: International Renewable Energy Agency; 2022.

[16] Badrinarayanan DSR, Bokkassam SD, Krishnan JN. Investigation on implementing hydrogen technology in residential sector. Energy Rep 2024;12:920–41. https://doi.org/10.1016/j.egyr.2024.07.005.

[17] World Energy Transitions Outlook 2023: 1.5°C pathway. International Renewable Energy Agency (IRENA), Abu Dhabi; 2023. https://www.irena.org/Publications/2023/Jun/World-Energy-Transitions-Outlook-2023.

[18] Renewable power generation costs in 2023. International renewable energy agency (IRENA), Abu Dhabi. https://www.irena.org/-/media/Files/IRENA/Agency/Publication/2024/Sep/IRENA_Renewable_power_generation_costs_in_2023.pdf; 2024.

[19] World Energy Outlook 2024. Paris: International Energy Agency (IEA); 2024. https://www.iea.org/reports/world-energy-outlook-2024.

[20] Photovoltaics Report. Fraunhofer Institute for solar energy systems ISE. https://www.ise.fraunhofer.de/en/publications/studies/photovoltaics-report.html. [Accessed 20 October 2024].

[21] Weiss W, Spörk-Dür M. Solar heat worldwide 2024. IEA SHC 2024. https://doi.org/10.18777/ieashc-shww-2024-0001.

[22] Dupeyrat P, Ménézo C, Fortuin S. Study of the thermal and electrical performances of PVT solar hot water system. Energ Build 2014;68:751–5. https://doi.org/10.1016/j.enbuild.2012.09.032.

[23] Madurai Elavarasan R, Mudgal V, Selvamanohar L, Wang K, Huang G, Shafiullah GM, et al. Pathways toward high-efficiency solar photovoltaic thermal management for electrical, thermal and combined generation applications: a critical review. Energy Convers Manag 2022;255:115278. https://doi.org/10.1016/j.enconman.2022.115278.

[24] Herrando M, Wang K, Huang G, Otanicar T, Mousa OB, Agathokleous RA, et al. A review of solar hybrid photovoltaic-thermal (PV-T) collectors and systems. Prog Energy Combust Sci 2023;97:101072. https://doi.org/10.1016/j.pecs.2023.101072.

[25] Lämmle M, Herrando M, Ryan G. Basic concepts of PVT collector technologies, applications and markets. In: IEA SHC Task 60; 2020. https://doi.org/10.18777/ieashc-task60-2020-0002.

[26] Kamel RS, Fung AS, Dash PRH. Solar systems and their integration with heat pumps: a review. Energ Build 2015;87:395–412. https://doi.org/10.1016/j.enbuild.2014.11.030.

[27] Poppi S, Sommerfeldt N, Bales C, Madani H, Lundqvist P. Techno-economic review of solar heat pump systems for residential heating applications. Renew Sust Energ Rev 2018;81:22–32. https://doi.org/10.1016/j.rser.2017.07.041.

[28] Sezen K, Tuncer AD, Akyuz AO, Gungor A. Effects of ambient conditions on solar assisted heat pump systems: a review. Sci Total Environ 2021;778:146362. https://doi.org/10.1016/j.scitotenv.2021.146362.

[29] Najjaran Kheirabadi A, Harraz AA, Freeman J, Mac Dowell N, Markides CN. Numerical and experimental investigations of diffusion absorption refrigeration systems for use with low temperature heat sources. In: ECOS 2018 - 31st Int. Conf. Effic. Cost Optim. Simul. Environ. Impact Energy Syst. ECOS; 2018. http://spiral.imperial.ac.uk/handle/10044/1/62182. [Accessed 14 November 2024].

[30] Harraz AA, Freeman J, Wang K, Dowell NM, Markides CN. Diffusion-absorption refrigeration cycle simulations in gPROMS using SAFT-γ Mie. Energy Procedia 2019;158:2360–5. https://doi.org/10.1016/j.egypro.2019.01.284.

[31] Mungyeko Bisulandu B-JR, Mansouri R, Ilinca A. Diffusion absorption refrigeration systems: an overview of thermal mechanisms and models. Energies 2023;16:3610. https://doi.org/10.3390/en16093610.

[32] Lima AAS, Leite GDNP, Ochoa AAV, Santos CACD, Costa JAPD, Michima PSA, et al. Absorption refrigeration systems based on Ammonia as refrigerant using different absorbents: review and applications. Energies 2020;14:48. https://doi.org/10.3390/en14010048.

[33] Ala G, Orioli A, Di Gangi A. Energy and economic analysis of air-to-air heat pumps as an alternative to domestic gas boiler heating systems in the south of Italy. Energy 2019;173:59–74. https://doi.org/10.1016/j.energy.2019.02.011.

[34] Emmi G, Tisato C, Zarrella A, De Carli M. Multi-source heat pump coupled with a photovoltaic thermal (PVT) hybrid solar collectors Technology: a case study in residential application. Int J Energy Prod Manag 2016;1:382–92. https://doi.org/10.2495/EQ-V1-N4-382-392.

[35] Wang K, Herrando M, Pantaleo AM, Markides CN. Technoeconomic assessments of hybrid photovoltaic-thermal *vs.* conventional solar-energy systems: case studies in heat and power provision to sports centres. Appl Energy 2019;254:113657. https://doi.org/10.1016/j.apenergy.2019.113657.

[36] Panagiotidou M, Aye L, Rismanchi B. Solar driven water heating systems for medium-rise residential buildings in urban mediterranean areas. Renew Energy 2020;147:556–69. https://doi.org/10.1016/j.renene.2019.09.020.

[37] Energetic analysis using theoretical modeling and the characteristic equation method in a small absorption chiller with LiBr/H_2O, Acta. Sci Technol 2018;40. https://doi.org/10.4025/actascitechnol.v40i1.34969. e34969–e34969.

[38] Thygesen R, Karlsson B. Simulation and analysis of a solar assisted heat pump system with two different storage types for high levels of PV electricity self-consumption. Sol Energy 2014;103:19–27. https://doi.org/10.1016/j.solener.2014.02.013.

[39] Inc MathWorks. MATLAB. https://www.mathworks.com; 2023.

[40] Lemmon Eric W, Bell Ian H, Huber Marcia L, McLinden Mark O. NIST standard reference database 23: Reference fluid thermodynamic and transport properties-REFPROP. 2018.

[41] International Organization for Standardization. EN ISO 9806:2017 - Solar energy – Solar thermal collectors – Test methods. 2017.

[42] Evans DL, Florschuetz LW. Cost studies on terrestrial photovoltaic power systems with sunlight concentration. Sol Energy 1977;19:255–62. https://doi.org/10.1016/0038-092X(77)90068-8.

[43] Heydenreich W, Müller B, Reise C. Describing the world with three parameters: A new approach to PV module power modelling. In: 23rd Eur. Photovolt. Sol. Energy Conf. Exhib.; 2008. https://doi.org/10.4229/23RDEUPVSEC2008-4DO.9.4.

[44] Dubey S, Sarvaiya JN, Seshadri B. Temperature dependent photovoltaic (PV) efficiency and its effect on PV production in the world – a review. Energy Procedia 2013;33:311–21. https://doi.org/10.1016/j.egypro.2013.05.072.

[45] Herrando M, Ramos A, Freeman J, Zabalza I, Markides CN. Technoeconomic modelling and optimisation of solar combined heat and power systems based on flat-box PVT collectors for domestic applications. Energy Convers Manag 2018;175:67–85. https://doi.org/10.1016/j.enconman.2018.07.045.

[46] Duffie John A, Beckman William A. Solar engineering of thermal processes. 4th ed. John Wiley & Sons, Ltd; 2013. https://doi.org/10.1002/9781118671603.

[47] Jones AD, Underwood CP. A thermal model for photovoltaic systems. Sol Energy 2001;70:349–59. https://doi.org/10.1016/S0038-092X(00)00149-3.

[48] Olympios AV, Pantaleo AM, Sapin P, Markides CN. On the value of combined heat and power (CHP) systems and heat pumps in centralised and distributed heating systems: lessons from multi-fidelity modelling approaches. Appl Energy 2020;274:115261. https://doi.org/10.1016/j.apenergy.2020.115261.

[49] Olympios AV, Hoseinpoori P, Mersch M, Pantaleo AM, Simpson M, Sapin P, et al. Optimal design of low-temperature heat-pumping technologies and implications to the whole- energy system. In: Osaka, Japan; 2020.

[50] Olympios AV, Mersch M, Sapin P, Pantaleo AM, Markides CN. Library of price and performance data of domestic and commercial technologies for low-carbon energy systems. 2021. https://doi.org/10.5281/zenodo.4692649.

[51] BITZER Kühlmaschinenbau GmbH. Refrigerant Report - Quick Guide. Germany: Sindelfingen; 2023. https://www.bitzer.de/shared_media/images/topic-stories/2023_refrigerants/part2/Refrigerant-Report-Quick-Guide_2023-10-23.pdf.

[52] Kropp M, Lämmle M, Herkel S, Henning H-M, Velte-Schäfer A. Enhancing heat pump performance for domestic hot water preparation: a comparative analysis in existing multi-family houses. Energ Build 2025;328:115155. https://doi.org/10.1016/j.enbuild.2024.115155.

[53] Terhan M, Comakli K. Energy and exergy analyses of natural gas-fired boilers in a district heating system. Appl Therm Eng 2017;121:380–7. https://doi.org/10.1016/j.applthermaleng.2017.04.091.

[54] Nikbakhti R, Wang X, Hussein AK, Iranmanesh A. Absorption cooling systems – review of various techniques for energy performance enhancement. Alex Eng J 2020;59:707–38. https://doi.org/10.1016/j.aej.2020.01.036.

[55] Altamirano A, Pierrès NL, Stutz B. Review of small-capacity single-stage continuous absorption systems operating on binary working fluids for cooling: theoretical, experimental and commercial cycles. Int J Refrig 2019;106:350–73. https://doi.org/10.1016/j.ijrefrig.2019.06.033.

[56] Siller DA, Anderson K. J.J. Shepherd. ASHRAE Position Document on Ammonia as a Refrigerant. 2025. n.d.

[57] Harraz A. Computer-aided molecular and system Design of Diffusion Absorption Solar-Cooling Systems. PhD thesis. Imperial College London, Department of Chemical Engineering; 2022. https://spiral.imperial.ac.uk/entities/publication/350ab9d5-0f7a-424a-b449-3f1da91f3bac.

[58] Turton R, editor. Analysis, synthesis, and design of chemical processes. 4th ed. Upper Saddle River, NJ: Prentice Hall; 2012.

[59] Jensen Jørgen Bauck, Skogestad Sigurd. Problems with specifying ΔT_{min} in the Design of Processes with heat exchangers | Industrial & Engineering Chemistry Research. Ind Eng Chem Res 2008;47:3071–5. https://doi.org/10.1021/ie071335t.

[60] Khorasaninejad E, Hajabdollahi H. Thermo-economic and environmental optimization of solar assisted heat pump by using multi-objective particle swam algorithm. Energy 2014;72:680–90. https://doi.org/10.1016/j.energy.2014.05.095.

[61] European Commission (2024) *Report from the Commission to the European Parliament and the Council: 2024 Carbon Market Report*. Available at: https://climate.ec.europa.eu/document/download/92ec0ab3-24cf-4814-ad59-81c15e310bea_en?filename=2024_carbon_market_report_en.pdf.

[62] Haimes G. Carbon pricing rapidly gaining 'much needed' traction in real estate, say ULI and PwC, ULI Eur. https://europe.uli.org/carbon-pricing-rapidly-gaining-much-needed-traction-in-real-estate-say-uli-and-pwc/. [Accessed 18 November 2024].

[63] BS EN 14825:2022 - Air Conditioners. Liquid Chilling Packages, and Heat Pumps. 2022.
[64] JRC Photovoltaic Geographical Information System (PVGIS) - European Commission (n.d.), https://re.jrc.ec.europa.eu/pvg_tools/en/. [Accessed 2 January 2025].
[65] Ruhnau O, Hirth L, Praktiknjo A. Time series of heat demand and heat pump efficiency for energy system modeling. Sci Data 2019;6:189. https://doi.org/10.1038/s41597-019-0199-y.
[66] Pezzutto PS, Zambotti S, Croce S, Zambelli P, Scaramuzzino C, Pascuas RP, et al. Open Data Set for the EU28. n.d. https://www.hotmaps-project.eu/wp-content/uploads/2018/03/D2.3-Hotmaps_for-upload_revised-final_.pdf; 2025.
[67] Energy Efficiency by Sector – Households. ODYSSEE-MURE. n.d. https://www.odyssee-mure.eu/publications/efficiency-by-sector/households/. [Accessed 17 November 2024].
[68] ENTSO-E, ENTSO-E Transparency Platform. n.d. https://transparency.entsoe.eu/. [Accessed 17 November 2024].
[69] Electricity Maps. n.d. https://www.electricitymaps.com/data-portal. [Accessed 17 November 2024].
[70] Methodology | Electricity Maps. n.d. https://www.electricitymaps.com/methodology. [Accessed 25 May 2025].
[71] Pachauri Rajendra K, Allen Myles R, Barros Vicente R, Broome John, Cramer Wolfgang, Christ Renate, et al. Intergovernmental Panel on Climate Change, eds., Climate change 2014: Synthesis report. In: Contribution of working groups I, II and III to the fifth assessment report of the intergovernmental panel on climate change, Intergovernmental Panel on Climate Change, Geneva, Switzerland; 2015.
[72] Bódis K, Kougias I, Jäger-Waldau A, Taylor N, Szabó S. A high-resolution geospatial assessment of the rooftop solar photovoltaic potential in the European Union. Renew Sust Energ Rev 2019;114:109309. https://doi.org/10.1016/j.rser.2019.109309.
[73] Byrne J, Taminiau J, Kurdgelashvili L, Kim KN. A review of the solar city concept and methods to assess rooftop solar electric potential, with an illustrative application to the city of Seoul. Renew Sust Energ Rev 2015;41:830–44. https://doi.org/10.1016/j.rser.2014.08.023.
[74] Yang Y, Campana PE, Stridh B, Yan J. Potential analysis of roof-mounted solar photovoltaics in Sweden. Appl Energy 2020;279:115786. https://doi.org/10.1016/j.apenergy.2020.115786.
[75] Potential for building integrated photovoltaics. International Energy Agency; 2002. https://iea-pvps.org/wp-content/uploads/2020/01/rep7_04.pdf [accessed March 21, 2025].
[76] Defaix PR, van Sark WGJHM, Worrell E, de Visser E. Technical potential for photovoltaics on buildings in the EU-27. Sol Energy 2012;86:2644–53. https://doi.org/10.1016/j.solener.2012.06.007.
[77] Koch H, Lechner S, Erdmann S, Hofmann M. Assessing the potential of rooftop photovoltaics by processing high-resolution irradiation data, as applied to Giessen, Germany. Energies 2022;15:6991. https://doi.org/10.3390/en15196991.
[78] Big Four make price promise on domestic hydrogen boilers. The Engineer; 2021. https://www.theengineer.co.uk/content/news/big-four-make-price-promise-on-domestic-hydrogen-boilers/. [Accessed 13 March 2025].
[79] Annual average price of European Union Emissions Trading System (EU ETS) allowances from 2020 to 2024. Statista 2025. https://www.statista.com/statistics/1465687/average-annual-eu-ets-allowance-prices/.
[80] Statistics | Eurostat. n.d. https://ec.europa.eu/eurostat/databrowser/view/nrg_pc_204/default/table?lang=en. [Accessed 17 November 2024].
[81] Market Price Electricity | Helen. https://www.helen.fi/en/electricity/electricity-products-and-prices/marketpriceelectricity. [Accessed 17 November 2024].
[82] France unveils new FIT rates for PV systems up to 500 kW, Pv Mag. Int.. https://www.pv-magazine.com/2023/03/01/france-unveils-new-fit-rates-for-pv-systems-up-to-500-kw/; 2023.
[83] Greece adds storage to solar tenders, Pv Mag. Int.. https://www.pv-magazine.com/2024/05/27/greece-adds-storage-to-solar-tenders/; 2024.
[84] Tilastokeskus. Statistics Finland. n.d. https://stat.fi/tup/tilastotietokannat/index_en.html. [Accessed 17 November 2024].
[85] Annual inflation up to 2.6% in the euro area. https://ec.europa.eu/eurostat/web/products-euro-indicators/w/2-20082024-ap. [Accessed 17 November 2024].
[86] Reference and discount rates - European Commission. n.d. https://competition-policy.ec.europa.eu/state-aid/legislation/reference-discount-rates-and-recovery-interest-rates/reference-and-discount-rates_en. [Accessed 17 November 2024].
[87] Juhrich K. CO_2 -Emissionsfaktoren für fossile Brennstoffe. Umweltbundesamt, Dessau-Roßlau; 2022. https://www.umweltbundesamt.de/publikationen/co2-emissionsfaktoren-fuer-fossile-brennstoffe-0.
[88] Energy Box. Energy-Box. https://www.energy-box.com/post/france-updates-fit-rates-for-photovoltaic-systems-up-to-500kw. [Accessed 10 January 2025].
[89] Tselepis S. The PV market developments in Greece, feed-in-premium scheme. In: Center for Renewable Energy Sources and Saving (CRES); 2004.
[90] National Survey Report of PV Power Applications in FINLAND. International energy agency photovoltaic power systems Programme (IEA PVPS), Paris, France. https://iea-pvps.org/wp-content/uploads/2020/09/NSR_Finland_2019.pdf; 2016.
[91] Clean Hydrogen Monitor. Hydrogen Europe. https://hydrogeneurope.eu/wp-content/uploads/2023/10/Clean_Hydrogen_Monitor_11-2023_DIGITAL.pdf#page=43.08; 2023.
[92] PricewaterhouseCoopers. Green hydrogen economy - predicted development of tomorrow. PwC; 2025. n.d. https://www.pwc.com/gx/en/industries/energy-utilities-resources/future-energy/green-hydrogen-cost.html. [Accessed 29 November 2024].
[93] Hybrid solar panel Ecomesh. n.d. https://endef.com/en/hybrid-solar-panel/ecomesh/. [Accessed 2 January 2025].
[94] UL-355-120 data sheet. https://www.sents.nl/wp-content/uploads/2020/07/UL-355WP-120-BK-revisie-0.pdf. [Accessed 10 January 2025].
[95] SOLAR. 4000 TF | Solar-Flachkollektoren. n.d. https://www.bosch-homecomfort.com/de/de/ocs/wohngebaeude/solar-4000-tf-854607-p/. [Accessed 10 January 2025].
[96] Herrando M, Ramos A, Zabalza I, Markides CN. A comprehensive assessment of alternative absorber-exchanger designs for hybrid PVT-water collectors. Appl Energy 2019;235:1583–602. https://doi.org/10.1016/j.apenergy.2018.11.024.
[97] Herrando M, Markides CN. Hybrid PV and solar-thermal systems for domestic heat and power provision in the UK: techno-economic considerations. Appl Energy 2016;161:512–32. https://doi.org/10.1016/j.apenergy.2015.09.025.
[98] Pino A, Javier Pino F, Cabello González G, Navas SJ, Guerra J. PVT potential for a small-scale brewing process: a case study. Therm Sci Eng Prog 2024;53:102670. https://doi.org/10.1016/j.tsep.2024.102670.
[99] BOSCH. Sonnenkollektor SO4000 TFV -FCC220-2V Flachkollektor senkrecht, 2026x1032x67 | 1917872. Haustech: Altern; 2025. n.d. https://www.alternative-haustechnik.de/bosch-sonnenkollektor-so4000-tfv-fcc220-2v-flachkollektor-senkrecht-2026x1032x67/1917872. [Accessed 24 March 2025].
[100] European Heat Pump Association. EHPA heat pump market and statistic Report 2024. Brussels: EHPA; 2024. https://www.ehpa.org/wp-content/uploads/2024/08/Executive-summary_EHPA-heat-pump-market-and-statistic-report-2024-2.pdf.
[101] Rogers GFC, Mayhew YR. Heat transfer and pressure loss in helically coiled tubes with turbulent flow. Int J Heat Mass Transf 1964;7:1207–16. https://doi.org/10.1016/0017-9310(64)90062-6.
[102] Fernández-Seara J, Diz R, Uhia FJ, Sieres J, Dopazo A. Thermal analysis of a helically coiled tube in a domestic hot water storage tank. In: International Conference on Heat Transfer, Fluid Mechanics and Thermodynamics; 2007. https://repository.up.ac.za/handle/2263/45760. [Accessed 18 November 2024].
[103] Schmidt EF. Wärmeübergang und Druckverlust in Rohrschlangen. Chem Ing Tech 1967;39:781–9. https://doi.org/10.1002/cite.330391302.
[104] Bellos V, Nalbantis I, Tsakiris G. Friction modeling of flood flow simulations. J Hydraul Eng 2018;144:04018073. https://doi.org/10.1061/(ASCE)HY.1943-7900.0001540.
[105] Kovacs P, Persson M, Wahlgren P, Jensen S. Pressure drop over a solar flat plate collector using various heat transfer fluids. Technical Research Institute of Sweden; 2012.
[106] Herrando M, Markides CN, Hellgardt K. A UK-based assessment of hybrid PV and solar-thermal systems for domestic heating and power: system performance. Appl Energy 2014;122:288–309. https://doi.org/10.1016/j.apenergy.2014.01.061.
[107] Quoilin Sylvain, Declaye Sébastien, Tchanche Bertrand F, Lemort Vincent. Thermo-economic optimization of waste heat recovery organic Rankine cycles. Appl Therm Eng 2011;31:2885. https://doi.org/10.1016/j.applthermaleng.2011.05.014.
[108] Han H. Techno-economic assessment of solar combined heating and power systems for domestic applications in European countries: A comparative analysis. Master's Thesis,. Germany: Karlsruhe Institute of Technology; 2023.